

The Crystal/Liquid Interface: Structure and Properties from Computer Simulation

Brian B. Laird and A. D. J. Haymet*

Department of Physical and Theoretical Chemistry, University of Sydney, NSW 2006 Australia

Received June 25, 1992 (Revised Manuscript Received September 21, 1992)

Contents

I. Introduction	1819
II. Characterization of the Interface	1819
A. Thermodynamics	1819
B. Structure and Dynamics	1821
III. Simulation of Interfaces	1822
A. Simulation Techniques	1822
B. Construction of an Equilibrium Interface	1822
C. Thermodynamic Averages	1823
IV. Predicted Quantities for Simple Systems	1823
A. Hard Spheres	1823
B. Inverse-Power Potentials	1824
C. The Lennard-Jones Potential	1826
V. Results for More Complex Systems	1829
A. The Ice/Water Interface	1829
B. The Silicon Interface	1832
VI. Theory of the Crystal/Liquid Interface	1833
VII. Summary	1836

I. Introduction

The physical nature of an interface between a crystal and its melt are of paramount importance in the study of crystal growth near equilibrium and homogeneous nucleation. Such an interface lies between two condensed phases, which makes direct experimental study difficult.¹ Quantities of interest are *thermodynamic*, such as the crystal/liquid interfacial free energy γ_{cl} , *structural*, for example the microscopic density profile in the interfacial region, and *dynamic*, such as the variation of the molecular self-diffusion constant through the interfacial region.

Laboratory estimates of the surface tension for a limited number of systems have been obtained both directly²⁻⁶ and indirectly.⁷ However, experimental data concerning the microscopic structure and dynamics of the interfacial region is lacking. This experimental difficulty increases the importance of computer simulations in the microscopic study of such interfacial phenomena.

In this review, we will survey recent progress in the simulation of the interface between a crystal and its own melt. We concentrate on studies that have appeared since the definitive review of Bonissent.⁸ To date, there have been approximately 20 such simulations of a variety of atomic and molecular systems. Relaxation of the crystal phase in the vicinity of the boundary with the liquid plays a very important role in determining the structure of interfacial region. Hence, only simulations that allow for such relaxation will be

considered here; that is, we omit discussion of simulations of a fluid up against a structured or structureless wall, which may be important in other applications. In addition, since our focus is on the properties of an equilibrium interface, simulations that are concerned entirely with nonequilibrium interfaces will not be discussed.

We begin in section II with a background discussion of the various thermodynamic, structural, and dynamical quantities that describe an interface between a crystal and its melt. The determination of these quantities from a computer simulation of a specific interface is described in section III. The results of simulations for simple systems, such as hard spheres and inverse power and Lennard-Jones potentials, are collected in section IV, and for the complex systems water and silicon in section V. In section VI, we outline the current level of theories of the crystal/liquid interface, and summarize the review in section VII.

II. Characterization of the Interface

A. Thermodynamics

The formal mathematical framework characterizing the thermodynamics of an interface between coexisting phases was developed by J. W. Gibbs in the late 19th century.⁹ Central to this formalism is the realization that all the excess thermodynamic properties of the interfacial region can be assigned arbitrarily to a mathematical *dividing surface*, separating the two phases. Thus, all thermodynamic quantities of the two-phase system may be written as the sum of two bulk contributions, calculated as if each bulk phase were uniform up to the Gibbs dividing surface, plus an excess term due to the presence of the interface. For example, for a general multicomponent system consisting of two phases, denoted by 1 and 2, in equilibrium separated by a flat interface, the extensive thermodynamic properties may be written

$$E = E_1 + E_2 + E_{12} \quad (1)$$

$$V = V_1 + V_2 + V_{12} \quad (2)$$

$$S = S_1 + S_2 + S_{12} \quad (3)$$

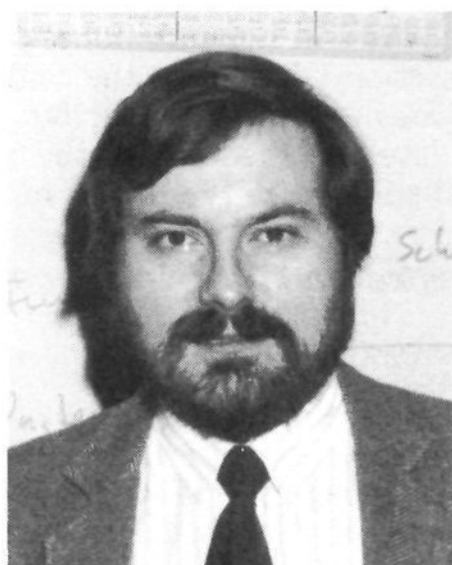
$$N^i = N_1^i + N_2^i + N_{12}^i \quad (4)$$

where E , V , S , and N^i are the energy, volume, entropy, and number of particles of type i , respectively.

Defining the excess interfacial free energy, γ , to be the work necessary to form a unit area of interface, the



Brian Laird was born in Port Arthur, TX, on August 16, 1960. He received B.S. degrees in Chemistry and Mathematics from the University of Texas at Austin in 1982. He then attended the University of California at Berkeley, where he received a Ph.D. in theoretical chemistry in 1987 in the group of Prof. A. D. J. Haymet. After a year and a half as a postdoctoral associate in the group of Prof. James Skinner at Columbia University, Dr. Laird, was awarded a NATO Postdoctoral Fellowship, which he spent at the Institut für Festkörperforschung des Forschungszentrum in Jülich, Germany. He is currently a research associate with Prof. A. D. J. Haymet at the University of Sydney. His research interests include first-order phase transitions, interfaces, inhomogeneous fluids, low-temperature properties of glasses, and relaxation and transport of excitations in condensed matter.



Tony Haymet is Professor of Theoretical Chemistry at the University of Sydney. He obtained a B.Sc. with first class honors, and the University Medal in Theoretical Chemistry, from the University of Sydney in 1978, and a Ph.D. in Chemistry from the University of Chicago in 1981. After 2 years of postdoctoral research in the Physics Department at Harvard University, he taught for 5 years at the University of California, Berkeley, and 3 years at the University of Utah before returning to Sydney in August 1991. Professor Haymet is the recipient of the U.S. Presidential Young Investigator Award (1985–90), an Alfred P. Sloan Foundation Fellowship (1986), and the Rennie (1988) and Masson (1976) Medals of the Royal Australian Chemical Institute. He has published over 80 papers in the statistical mechanics of liquids, freezing, interfaces, and chemical reactions in solution. Professor Haymet is best known for his work on theories of freezing and interfaces. In recent years he has focused on chemical reactions in solution, developing new integral equations, simulation techniques, and methods for incorporating quantum degrees of freedom into otherwise classical systems. He has taught courses in Biophysical Chemistry, Introductory Chemistry, undergraduate Physical Chemistry, and graduate Thermodynamics and Statistical Mechanics. He has supervised the research of seven Ph.D. students. He has worked with 10 postdoctoral researchers, and has a worldwide network of collaborators from Ukraine, Slovenia, Mexico, Canada, Spain, Sweden, and Australia.

Euler equation for the total energy becomes

$$E = TS - PV + \sum_i \mu_i N^i + \gamma A \quad (5)$$

where A is the area of the interface. Since the excess

interfacial volume is zero by definition, the corresponding Euler equation for the excess interfacial quantities is

$$\epsilon = T\eta + \sum_i \mu_i \Gamma^i + \gamma \quad (6)$$

where ϵ , η , and Γ^i are the excess energy, excess entropy, and excess number of type i particles, all measured per unit area. Rearranging eq 6 yields

$$\gamma = \epsilon - T\eta - \sum_i \mu_i \Gamma^i \quad (7)$$

Defining the excess Helmholtz free energy per unit area via $f = \epsilon - T\eta$, yields

$$\gamma = f - \sum_i \mu_i \Gamma^i \quad (8)$$

For a single-component system, Gibbs recognized that eq 8 could be simplified by choosing the position of the dividing surface such that the excess number of particles is zero ($\Gamma = 0$) so that

$$\gamma = f \quad (9)$$

For a multicomponent system, such a simplification is not possible in general, due to the differential adsorption of the various components at the interface. If one of the components can be identified as the "solvent", it is convenient to define the Gibbs dividing surface so that the excess concentration of this species vanishes. The surface excess particle densities of the remaining components may be determined from the Gibbs adsorption isotherm (the differential version of eq 7)

$$\Gamma^i = \left(\frac{\partial \gamma}{\partial \mu_i} \right)_{T,P,\mu_j} \quad (10)$$

It should be noted that the excess interfacial free energy γ is invariant to the specific location of the Gibbs dividing surface; however, the relative magnitudes of the energy, entropy and particle adsorption contributions to γ will depend greatly on this choice.

As defined, the interfacial free energy γ is the work required in *forming* a unit area of interface. The work required to create a unit area of interface by *stretching* is known as the surface tension or surface stress and is, in general, a second-rank tensor, σ_{ij} . (Often in the literature the term surface tension is used as a synonym for the interfacial free energy. The terminology used here is due to Gibbs.) The difference in these two quantities depends on the ability of the bulk phases to resist strain. In general, the surface stress is given by¹⁰

$$\sigma_{ij} = \gamma \delta_{ij} + (\partial \gamma / \partial \epsilon_{ij}) \quad (11)$$

where δ_{ij} is the usual Kronecker delta and ϵ_{ij} is the ij component of the strain tensor.

For an interface between two fluid phases (liquid or vapor), the second term of eq 11 is zero because, as the strain is applied, particles can travel freely back and forth between the surface and bulk in such a way that the structure of the interface will remain unchanged. Thus, the surface free energy and surface stress are identical. For an interface with at least one crystal side, the approach to strict equilibrium is usually slow. The difference between the surface stress and the interfacial free energy depends upon the time scale of the strain process relative to the time scale of surface relaxation τ . For a crystal that is perfect except for

possible point defects, this relaxation time is infinite.¹⁰ At high temperatures near the melting point, the timescale τ is reduced greatly due to the presence of grain boundaries, which act as particle sources and sinks. If the experimental time scale is greater than the relaxation time τ , the equality of the surface free energy and surface stress can be assumed safely.¹ In simulations, however, this is not necessarily the case, due to the small size of the samples and the short total run times.

Experimentally, there are two basic approaches for determination of the crystal/liquid interfacial free energy γ_{cl} . The first assumes that classical nucleation theory is correct, and hence the free energy barrier to nucleation is a function of the surface free energy of the flat, infinite interface. Hence, measurements of the nucleation rate of supercooled liquids can be inverted to yield estimates of γ_{cl} . This has been performed for a variety of substances.⁷ Such methods are only as accurate as the theory that is used to perform the data inversion. Given the substantial approximations in even the best nucleation theories,¹¹ they are not quantitatively reliable in our opinion.

The second method is based on the fact that when three interfaces meet, the angles of intersection are determined by the various surface tensions via a force balance relation.¹ Such methods are free of the ambiguities inherent in the nucleation data inversions. For the crystal/liquid interface, Glicksman and Vold² developed a method to calculate γ_{cl} from the angle of the cusp formed at the intersection of a low-angle crystal grain boundary and the liquid phase. They used this method to determine the interfacial free energy of the bismuth interfaces and found it is relatively independent of interfacial orientation (index). Similar methods have been used to study a limited number of other systems, including water,³ succinonitrile,⁴ cadmium,⁵ and sodium chloride.⁶

B. Structure and Dynamics

The motion of each molecule in a crystal is restricted to a small region around a lattice site, leading to an average single-particle density $\rho(\mathbf{r})$ that is spatially periodic and inhomogeneous. (The drastic rearrangements that accompany vacancy diffusion in the crystal are an important exception.) However, from general symmetry arguments, the partition function of a multiparticle system in which the potential energy arises from interparticle interactions alone (that is, with a Hamiltonian which is invariant to translation and rotation of the entire system) must yield a uniform single-particle density. This apparent contradiction was resolved long ago by Kirkwood and Boggs,¹² who pointed out that in reality there are always external forces on the system (walls, etc.) which fix unambiguously the lattice position and orientation. Furthermore, the free energy cost for fixing the lattice position and orientation vanishes in the thermodynamic limit. In a liquid, on the other hand, $\rho(\mathbf{r})$ is uniform and isotropic, due to the random motions of each particle. When these two phases coexist, the structure in the neighborhood of the interface will relax to equilibrium. In the interfacial region, the single-particle density will have a structure intermediate between the two limiting bulk phases. Determining the width of this region is one of the prime goals of interfacial studies.

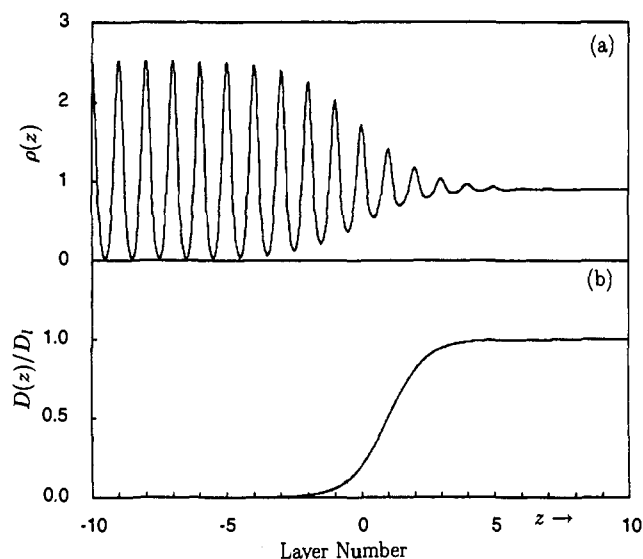


Figure 1. (a) Idealized interfacial density profile and (b) idealized interfacial diffusion profile (relative to the bulk liquid value D_l) versus layer number.

The decay of periodic density oscillations as one traverses the flat interface from the bulk crystal to the uniform bulk liquid is most easily visualized from plots of density profiles. Defining the coordinate perpendicular to the interface to be the z axis the density profile $\rho(z)$ is the average of the single-particle density over the directions (x and y) parallel to the surface

$$\rho(z) \equiv \langle \rho(\mathbf{r}) \rangle_{xy} \quad (12)$$

Figure 1a is a sketch of a typical density profile. For a polyatomic system such as water, where the molecules have orientational as well as translational degrees of freedom, profiles illustrating the decay of orientational order from the crystal to the liquid through the interfacial region are also important, since the length scale of this decay need not be the same as that for translational ordering. For polar systems, orientational order may persist for a significant distance into the bulk liquid phase long after the density oscillations have disappeared, due to the long-ranged nature of dipole forces compared to the relatively short-ranged interactions that govern packing and translational order.

Experimentally, the structure of interfaces between condensed phases are more difficult to study than the bulk substances, since traditional radiation probes are absorbed or scattered by one or both bulk phases. Techniques such as second harmonic generation (SHG) and ellipsometry have been useful in the study of some fluid/fluid¹³ or fluid/vapor interfaces¹⁴ and could, in principle, be used to study the crystal/fluid surface, but no such experiments have been published to our knowledge.

Near a crystal/liquid interface, the self-diffusion constant and other transport properties are altered from their bulk liquid values. For example, the self-diffusion constant in the bulk crystal is at least 1 (and often, several) order of magnitude smaller than the corresponding quantity in the bulk liquid. In the interfacial region, the diffusion constant will take on intermediate values. The width of this region is an important measure of the diffuseness of the interface. Figure 1b shows an idealized diffusion profile through the interface as a function of the perpendicular distance z . A

useful measure of the width of any quantity that varies continuously across the interfacial region is the so-called 10–90 width. For a given interfacial order parameter, this quantity is the distance over which the value of the parameter changes from 10% to 90% of its bulk solid value (relative to that of the bulk liquid) as one traverses the interface from liquid to solid. The 10–90 width of the diffusion profile shown in Figure 1b is about 4.9 lattice layers. Note that in simulations the self-diffusion constants for motion parallel and perpendicular to the interface are often measured separately, but do not appear to differ significantly from the isotropic value, at least in the studies to date.

The behavior of transport quantities near the interface plays a critical role in the kinetics of crystal growth from the melt. Propagation of the interfacial front requires both mass and latent heat transport between the bulk and surface regions. Despite the importance of these dynamical processes, little quantitative information is available. This current lack of experimental studies increases the usefulness of computer simulation.

III. Simulation of Interfaces

A. Simulation Techniques

Computer simulation techniques have become very important tools in the study of condensed-matter systems since their development in the 1950s. Such simulations can study systems ranging from the very simple (hard spheres, Lennard-Jones particles) to the complex (proteins and large biomolecules). The total number of atoms or molecules studied also varies greatly. For the calculation of the bulk properties of simple systems, a few hundred particles is usually sufficient. Other systems such as interfaces and proteins require much larger systems (thousands or perhaps tens of thousands of particles¹⁵). In the case of the crystal/liquid interface, simulations have a particularly important role because of the difficulty of performing experiments that probe the interface.

The techniques of computer simulation are divided into two major classes: Monte Carlo (MC) methods, developed by Metropolis, Rosenbluth, Rosenbluth, and Teller,¹⁶ and molecular dynamics (MD) methods, pioneered by Alder and Wainwright.¹⁷ The Monte Carlo technique uses random numbers to generate a set of configurations that are distributed according to the Boltzmann distribution (that is, $p\{\mathbf{R}\} \propto \exp[-\beta E(\{\mathbf{R}\})]$). The equilibrium value of any particular property is determined by averaging that property over the set of configurations. Because such a method uses *ensemble* averages instead of *time* averages, no direct information about transport quantities can be determined. On the other hand, a molecular dynamics simulation is the study of the time evolution of the dynamical state of a collection of interacting particles via numerical integration of the classical equations of motion. By performing averages over the resulting trajectories, most thermodynamic, structural, and *dynamical* properties of the system can be calculated. Because of the importance of interfacial diffusion processes to crystal growth, all simulations of crystal/liquid interfaces, with one exception, have used the molecular dynamics technique. Since many excellent references exist in the literature on the subject of computer simulations,¹⁸ only those aspects of the subject that are particular to

simulations of flat interfaces will be discussed here. It is assumed that the reader has at least a basic familiarity with molecular dynamics.

B. Construction of an Equilibrium Interface

The most difficult technical aspect of a crystal/liquid interface simulation is the construction of a stable equilibrium interface. Of course, the details of this process are irrelevant to the equilibrium properties discussed below in section IV, but it is an important technical point which we include here. The first step in this task is the determination of the conditions of coexistence, that is, the crystal and liquid densities at which the two phases will have the same temperature, pressure and chemical potential. The phase diagram can be obtained from either separate simulations of the bulk crystal and liquid phases,^{19–25} or by trial and error. These quantities must be determined accurately because any error will cause the interfacial system to be unstable to melting or crystallization during the simulation.

Once the freezing coexistence conditions are known, the interface can be built. The most generally applicable way of doing this is to first perform separate simulations of the bulk liquid and crystal phases at the appropriate coexistence temperature and densities. In order that these simulation cells will fit properly when placed together to form the interface, the *xy* cross-sectional area must be identical for both phases (where we define, as above, the *z* direction to be perpendicular to the interface). Due to the difference in density between the crystal and liquid phases, the equality of the cross-sectional area generally requires the liquid simulation cell to be noncubic with the *z*-axis dimension chosen to give the proper liquid density. After separate equilibration, the crystal and liquid blocks are placed end to end in the *z* direction to form the initial interface configuration. (To increase the size of the simulation, multiple copies of the crystal and liquid blocks may be used.) Periodic boundary conditions are then applied in all three Cartesian directions.

If the correct equations of motion were turned on at this point, the interface would not be stable because the liquid has not been equilibrated next to a crystal block. This results in high energy interactions at the interface, which when propagated melt the entire system. In order to create a stable interface, the following procedure may be adopted. First, the particles formerly in the crystal are held fixed while the particles formerly in the liquid are allowed to evolve for a sufficient number of simulation steps to reach equilibrium. In a molecular dynamics simulation the liquid temperature must also be rescaled periodically to the coexistence temperature. Hence in this step, energy is removed from the system to equilibrate the liquid next to a crystal with random but fixed displacements from the equilibrium lattice sites. Next, the particles formerly in the crystal are allowed to move (with their original velocities). The full system is then propagated until equilibrium is achieved. During the equilibration process it is important to monitor the temperature in various regions of the simulation cell to ensure that it is relatively uniform, that is, there are no hot or cold regions that indicate instability of the interface. Note that this method creates *two* independent crystal/liquid interfaces in the simulation cell. These can be compared

to give a measure of the statistical fluctuations in the simulation results.

Other methods to construct a crystal/liquid interface are possible. For example, for systems that are to be simulated under triple-point (three-phase) conditions,^{26,27} a block of crystal can be constructed in a simulation box sandwiched in the z direction between regions of empty space. By keeping one-half of the crystal region fixed and heating the other so that it melts, a three-phase system can be constructed. If this process is done carefully enough the system should come to equilibrium so that the densities of the various phases adjust to the proper triple-point values. One advantage of this procedure is that the coexistence conditions need not be determined beforehand, but are byproducts of the calculation. The method is extremely limited, however by the fact that the only one point along the crystal/liquid phase coexistence line can be studied thusly. Also the method is not applicable to purely repulsive potentials, such as the inverse power interactions, which have only one fluid phase.

C. Thermodynamic Averages

Once an equilibrium interface is constructed, the relevant system averages can be calculated. The density profile defined above in eq 12 is calculated by dividing the system into a number of equally spaced bins along the direction perpendicular to the interface (z axis). Calculating the average number of particles in each bin and dividing by the volume of the bin yields the density profile. The width of the bins must be chosen small enough that the crystal density peaks can be resolved but large enough to give good statistics.

Calculation of the diffusion constant profile is more difficult. Again the system is divided into z -axis bins. In general, these bins must be larger than those used to calculate the density profile. The variation of the diffusion constant is determined by calculating the average mean-squared displacement as a function of time for the particles assigned to each bin. The diffusion constant for a given bin is then calculated from the Einstein relation

$$D = \lim_{t \rightarrow \infty} \frac{\langle [\mathbf{r}(t) - \mathbf{r}(0)]^2 \rangle}{6kt} \quad (13)$$

using a least squares linear regression to calculate the slope of the mean-squared displacement curve. In order to guarantee the validity of this "course-graining" procedure, care must be taken to ensure that the bin spacing is large enough to minimize the effect of particles moving outside their assigned bin during the course of the mean-squared displacement measurement. In some calculations, authors have completely removed from the statistical averages the effect of particles which cross bin boundaries. The diffusion profile may be measured using only the mean-squared displacement in the xy plane (in this case the factor 6 in eq 13 is replaced by 4). For the limited data available, the perpendicular diffusion profile is not significantly different than the full isotropic profile.²⁸ Generally the interfacial width of the diffusion profile is smaller than that of the density profile and is displaced toward the "liquid" side of the interface.

The most difficult interfacial quantity to calculate is the interfacial free energy. The surface stress is related

to the interfacial free energy but not identical to it (see eq 11 and accompanying discussion). One method to measure the surface stress involves integrating the difference in the components of the pressure tensor perpendicular and parallel to the interface:

$$\sigma = \int_{-\infty}^{\infty} dz \left[p_{zz} - \frac{1}{2}(p_{xx} + p_{yy}) \right] \quad (14)$$

From simulation data, the integrand in the above integral is generally small with large error bars, and hence the statistical error in σ is usually quite substantial.

To date, there is only one method that has been used to calculate the interfacial free energy directly. (Indirect estimates have been attempted by combining the excess interfacial potential energy ϵ with an approximation of the excess entropy η ,^{29,30} but with little success.) This direct method is due to Broughton and Gilmer,³¹ and uses the concept of "cleaving potentials". A cleaving potential is constructed so that as it is applied slowly, the system is "cleaved" into two parts along the z axis. The separation between the two parts is increased until it exceeds the range of interaction of the particles. By monitoring the energy during the cleaving process, the thermodynamic integration method can be used to determine the amount of work involved. To calculate the interfacial free energy, which is the work necessary to form a unit area of interface from the bulk systems, four steps are necessary: (1) a cleaving potential is used to cleave a bulk crystal sample; (2) a similar process is applied to a liquid sample; (3) one half of the liquid sample is replaced with the bulk crystal (these two phases are still separated by the cleaving potential); (4) the cleaving potential is slowly removed until the crystal and liquid phases are in interfacial equilibrium. The interfacial free energy is the sum of the work necessary to perform steps 1–4. This procedure is lengthy and complicated, but if done carefully can yield good statistics.

IV. Predicted Quantities for Simple Systems

A. Hard Spheres

For the hard sphere system there are no true simulations of the crystal/liquid interface. Studies on this system are based on extensions of the static model approach to the structure of liquids due to Bernal.³² The applications of such methods to the crystal/liquid interface have been described extensively in an earlier review,⁸ and we merely summarize the results here.

The Bernal approach assumes that the structure of a liquid can be well described by a dense random packing of hard spheres. The construction of random packing would then yield a "typical" instantaneous liquid configuration. Originally such models were constructed using physical objects such as ping-pong balls, but more recently computers have been employed to generate the static configurations.³³

A corresponding model of a crystal/liquid interface has been built by constructing a dense random packing of hard spheres in contact with an face-centered-cubic (fcc) (111) or hexagonal-close-packed (hcp) (0001) crystal face, both using physical objects³⁴ and by computer generation.³⁵ The hard-sphere interfaces so formed are narrow and exhibit a substantial density deficit at the interface, implying poor wetting of a close-

packed crystal face by the melt. However, these results have been shown to be artifacts of the static nature of the model by subsequent computer simulations on soft spheres and Lennard-Jones particles. The failure of such approaches underscores the important role of relaxation of the crystal phase in the formation of the equilibrium crystal/liquid interface.

B. Inverse-Power Potentials

Systems of particles interacting via pairwise additive, purely repulsive inverse-power potentials have played

$$\phi(r) = \epsilon(\sigma/r)^n \quad (15)$$

an important role in the study of first-order phase transitions both through theory^{36,37} and simulation.^{20-24,28} Packing considerations, which dominate the freezing process in simple systems, are related directly to the repulsive part of the potential energy. This series of potentials permits wide variation of the range of the repulsion—from very short ranged hard spheres ($n = \infty$) to the extremely long ranged one-component plasma (OCP) ($n = 1$).

An interesting feature of this set of potentials is the presence of a crystal/crystal-phase transition at intermediate values of n . For high values ($n > 7$) the body-centered-cubic (bcc) crystal is mechanically unstable with respect to shear, due to the fact that nearest neighbor interactions alone do not stabilize the relatively open bcc structure and the second nearest neighbor interactions are too weak for such short ranged potentials. Consequently, the only thermodynamically stable phase above the freezing density is the face-centered-cubic (fcc) crystal [or perhaps hexagonal-close-packed (hcp)]—a situation typical of materials such as argon.³⁸ At the other extreme, very long ranged potentials such as the OCP have stable bcc structures that are lower in energy at zero temperature than the corresponding fcc crystals, and hence in equilibrium only the bcc phase is observed above the freezing transition, although a metastable fcc phase is also detected in simulations.²⁴

For intermediate-ranged potentials ($3 < n < 7$), the bcc phase is no longer mechanically unstable, but the fcc phase is the lower energy structure. This ensures that fcc is thermodynamically more stable than bcc at low temperatures (and high densities). However, the bcc phase has a higher entropy than the fcc crystal. In the language of crystal-state physics, this is due to the presence of a large number of low-frequency shear modes in the phonon spectrum. (These shear modes are the same ones that become unstable for more repulsive potentials.) If the entropy difference between the two phases is great enough, then as the temperature is raised sufficiently above zero, it is possible that the free energy of the bcc crystal will become lower than the free energy of the (lower energy) fcc crystal. If this event occurs before the melting point is reached, then the bcc phase will be the equilibrium crystal structure at freezing, eventually giving way to the fcc phase in a crystal/crystal transition as the density is increased or the temperature is lowered. This feature of the phase diagram (liquid–bcc–fcc) is typical for metals such as iron and those of the alkali group.³⁸ As an example, the calculated pressure–temperature phase diagram of the inverse sixth power potential²⁵ is shown in Figure 2.

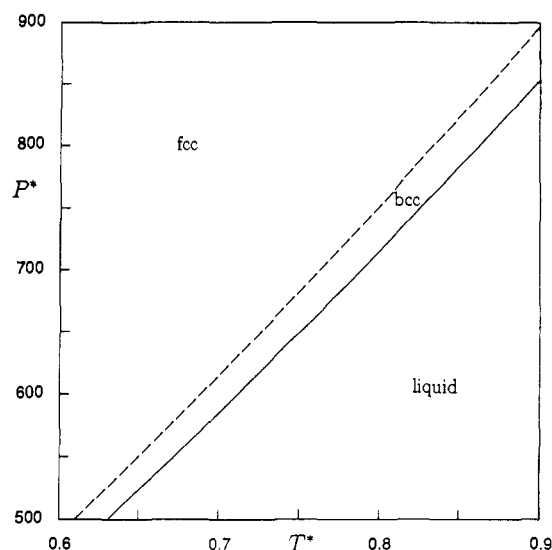


Figure 2. The pressure–temperature phase diagram of the inverse sixth power system. The temperature and pressure are in units of ϵ/k and ϵ/σ^3 , respectively. The regions of fcc crystal, bcc crystal, and liquid are labeled.

Note that stable phase at freezing is bcc, giving way to fcc at higher pressures and lower temperatures. The small extent of the bcc phase is an indication that this potential is near the border of bcc mechanical stability.

The first simulations of an inverse-power interface were performed on the fcc (100) crystal/liquid interface of an inverse twelfth power potential by Cape and Woodcock.^{39,40} The molecular dynamics technique was used to simulate a system of 7680 particles. The coexistence density and temperature chosen were identical (within statistical error) to those calculated in earlier studies of the bulk phases.^{20,22} The geometry of the system was such that each crystal plane parallel to the interface contained 128 particles. After equilibration, averages were calculated from a run of 900 time steps of $0.005 \sqrt{(m\sigma^2/\epsilon)}$.

Analysis of the density profile for this system yields an interface that is approximately about 6–7 lattice spacings wide. Plots of particle trajectories within individual layers in the interfacial region are also consistent with this value. The fraction of “liquidlike” particles in a given interface layer gradually increases as the bulk liquid is approached, while the mean square displacement of the “crystallike” particles increases. In the vicinity of the interface on the crystal side, there appears to be a slight expansion of the interlayer spacing of about 4% over the bulk value. The diffusion profile is measured from the slope of the layer-averaged mean-square displacement curves (eq 13) and gives a 10–90 width of about 5 lattice spacings, thus the interface width with respect to transport is smaller than that extracted from the structural data.

Cape and Woodcock also measured the interfacial surface stress from the difference between the components of the pressure tensor perpendicular and parallel to the interface. The calculated value of this quantity for the fcc (100) inverse twelfth power interface is $0.46 \pm 0.1(\epsilon/\sigma^2)(kT/\epsilon)^{7/6}$.

Subsequently Tallon⁴¹ investigated the fcc (111) interface of this same system by MD simulation of a system of 6480 particles. These simulations were undertaken primarily to study the layer structure of the interfacial region, which was found to be about five

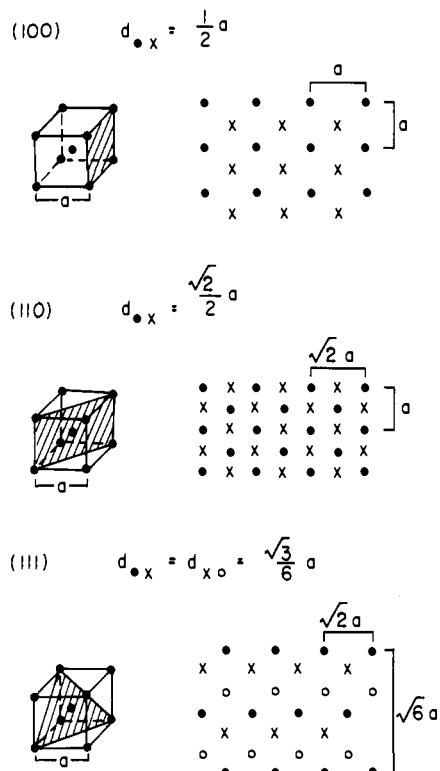


Figure 3. Definition of the (100), (110), and (111) interfaces from the bcc unit cell. The quantity $d_{\bullet x}$ is the distance between the \bullet and \times crystal planes for each interface. (Reprinted from ref 28. Copyright 1989 American Institute of Physics.)

(111) lattice layers wide. A Voronoi polygonal analysis of the individual layer structures was interpreted to show that the structure within a given layer was relatively homogeneous, namely that, "crystallike" or "liquidlike" domains do not coexist within the same layer.

The interfaces between an inverse-sixth-power crystal and its melt were studied by Laird and Haymet. These were the first such simulations involving body-centered-cubic (bcc) crystal faces. The motivation for such a study is that bcc is one of the simplest, commonly occurring, non-close-packed crystal structures and is a natural choice for extending the available simulation data beyond the close-packed systems. The sixth power was chosen because it is apparently the shortest range potential that freezes into a bcc crystal.^{23,25}

These simulations used the technique of constant energy and volume molecular dynamics using the velocity-Verlet algorithm of Swope.⁴² The bcc (100), (110), and (111) interfaces were simulated. (For reference, the details of the interfacial packing and the relationship to the bcc unit cell are illustrated for these three interfacial directions in Figure 3.) The values of the coexistence temperature and densities ($kT/\epsilon = 0.1$, $\rho_s\sigma^3 = 0.7$ and $\rho_l\sigma^3 = 0.687$) were chosen so that the system lies on the phase-coexistence line as estimated by simulation of the bulk properties of inverse-power potentials.²³ (Subsequent, more accurate simulations of inverse sixth power crystal/liquid freezing yielded slightly higher coexistence densities, but not different enough to affect the interfacial simulation results.²⁵)

The initial (100), (110), and (100) interfaces were each built from five blocks (three crystal and two liquid) of 686, 700, and 720 particles, respectively, yielding simulations of total particle number 3430, 3500, and

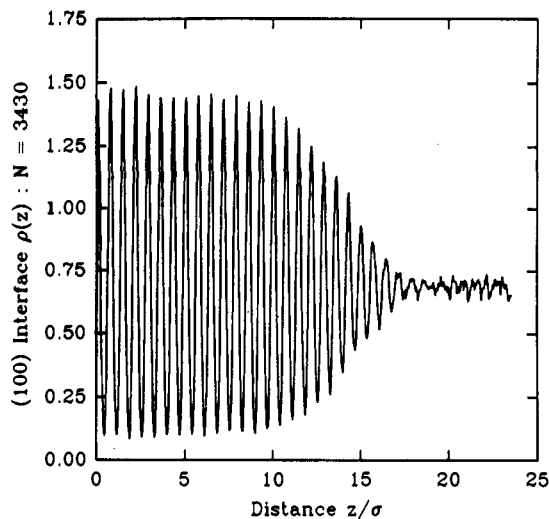


Figure 4. The reduced density profile $\sigma^3\rho(z)$, averaged over the perpendicular directions, of the $1/r^6$ equilibrium melt/bcc (100) crystal face, as a function of distance z/σ . (Reprinted from ref 28. Copyright 1989 American Institute of Physics.)

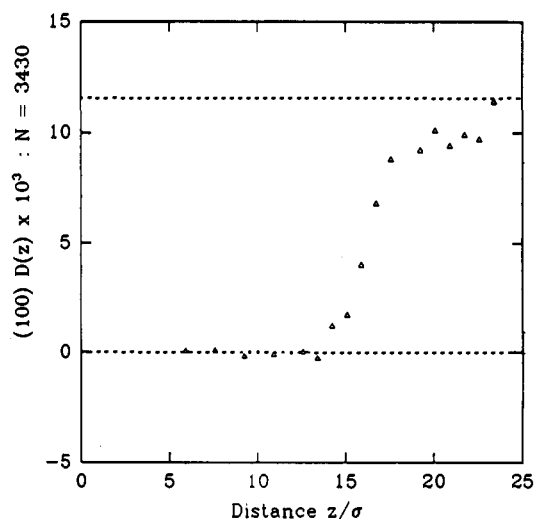


Figure 5. The measured diffusion constant $[(\epsilon\sigma^2/m)^{1/2} \times 10^3]$ in subregions of the $1/r^6$ bcc (100) interface. The upper dotted line is the equilibrium bulk liquid value. (Reprinted from ref 28. Copyright 1989 American Institute of Physics.)

3600, respectively. Once a stable interface was achieved, system averages were collected over 8000, 4000, and 16000 time steps for the (100), (110), and (111) interfaces, respectively. The disparity in the run times for the three interfaces is due primarily to the differences in the in-plane particle density (number of particles per unit cross-sectional area). The lower the number of particles per unit area in a given plane, the more time steps are required to generate acceptable statistics.

The calculated density profile for the (100) face is shown in Figure 4. The 10–90 width of the peak heights is just over nine lattice planes, which corresponds to about 6.4σ units. A comparison of this density profile with that of a previously simulated smaller system⁴³ with identical interfacial area shows that the two interfaces are essentially identical. The calculated (100) diffusion profile is shown in Figure 5. An eyeball estimate of the 10–90 width of the diffusion profile yields about 3.8σ or about five lattice plane spacings. Although the limiting bulk liquid diffusion constant values differ by about 10%, the values for the interface width are almost identical.

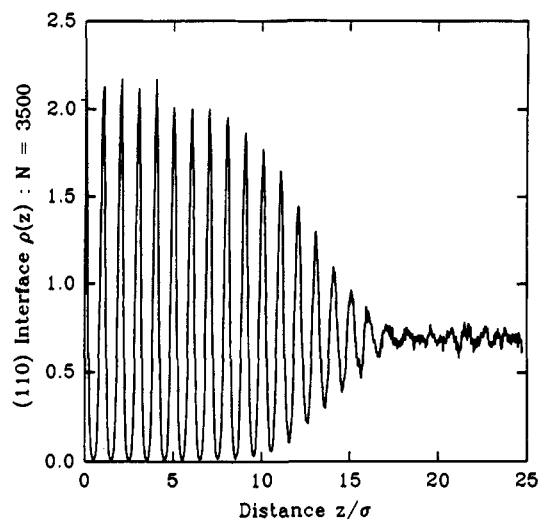


Figure 6. The reduced density profile $\sigma^3\rho(z)$, averaged over the perpendicular directions, of the $1/r^6$ equilibrium melt/bcc (110) crystal face, as a function of distance z/σ . (Reprinted from ref 28. Copyright 1989 American Institute of Physics.)

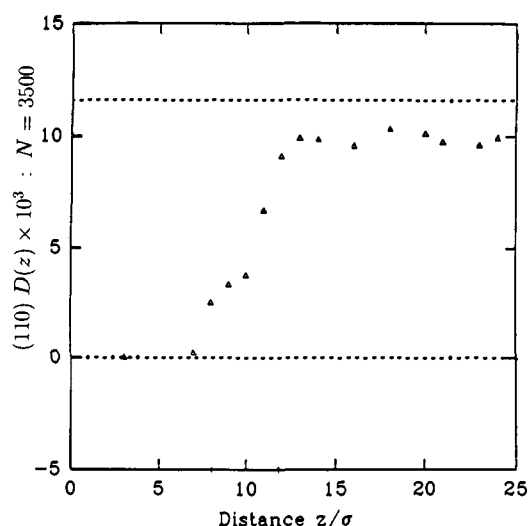


Figure 7. The measured diffusion constant $[(\epsilon\sigma^2/m)^{1/2} \times 10^3]$ in subregions of the $1/r^6$ bcc (110) interface. The upper dotted line is the equilibrium bulk liquid value. (Adapted from ref 28. Copyright 1989 American Institute of Physics.)

The density profile of the (110) interface is shown in Figure 6. The peak height 10–90 width for this interface is about 9.0σ (nine lattice planes), indicating a broader interfacial region than in the (100) simulation. The (110) diffusion profile is shown in Figure 7. A rough estimate of the diffusion 10–90 width yields 3.9σ or four bcc (110) lattice planes. This is almost exactly the same value as for the (100) interface, which is interesting in view of the fact that the density peak 10–90 widths for the two interfaces are very different.

Figure 8 shows the calculated (111) density profile. The peak height 10–90 width for the (111) interface is about 7.0σ (17 lattice planes). An interesting feature of the (111) density profile is that the *apparent* density between the lattice planes does not drop to zero. This is also the case for the (100) interface, although to a much lesser extent. This interplane density is *not* due to the diffusion of particles from one plane into the next, but rather reflects correctly the overlap of the z axis projections of the closely spaced (111) planes. The (111) crystal direction in the bcc crystal is made up of triangular lattice planes stacked upon each other, with the particles in each plane lying above the triangular

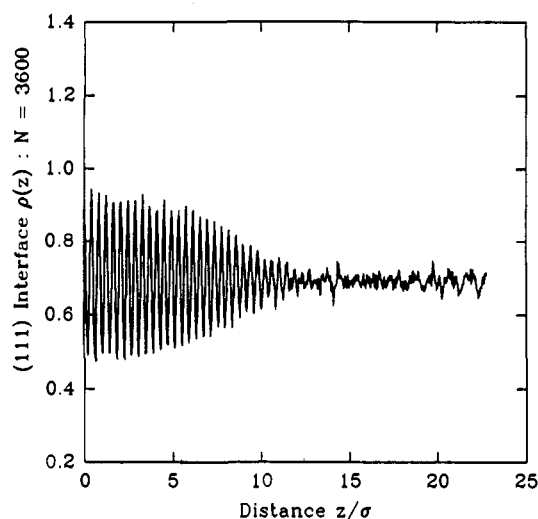


Figure 8. The reduced density profile $\sigma^3\rho(z)$, averaged over the perpendicular directions, of the $1/r^6$ equilibrium melt/bcc (111) crystal face, as a function of distance z/σ . (Reprinted from ref 28. Copyright 1989 American Institute of Physics.)

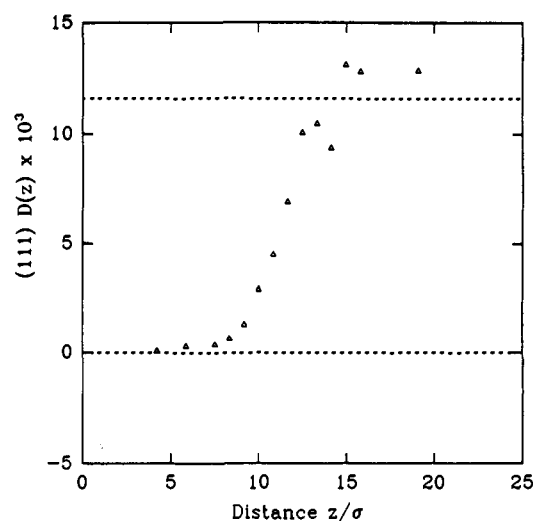


Figure 9. The measured diffusion constant $[(\epsilon\sigma^2/m)^{1/2} \times 10^3]$ in subregions of the $1/r^6$ bcc (111) interface. The upper dotted line is the equilibrium bulk liquid value. (Reprinted from ref 28. Copyright 1989 American Institute of Physics.)

holes of the previous plane in an ABCABC pattern. Since the spacing between the planes is quite small (about 0.41σ), the z coordinates of particles in two adjacent planes can overlap even though the particles remain localized about their respective lattice sites.

The diffusion profile for the (111) interface is shown in Figure 9. A rough estimate of the diffusion 10–90 width gives about 4.0σ or 10 (111) bcc lattice planes. Again it is interesting to note that this is almost exactly the same value as for the other two interfaces. It is therefore tempting to speculate that the differences in the density profiles among these three interfaces are due primarily to geometric considerations, which do not affect the transport properties. This lack of sensitivity of the diffusion width on the orientation of the interface has also been seen in the Lennard-Jones interfaces (discussed in the next section).

C. The Lennard-Jones Potential

Lennard-Jones (LJ) particles⁴⁴ interact via the spherically symmetric, pairwise-additive potential

$$\phi(r) = 4\epsilon[(\sigma/r)^{12} - (\sigma/r)^6] \quad (16)$$

where ϵ is the depth of the attractive well and σ is a measure of the particle size. This potential mimics the characteristics of the interaction potentials of rare gas elements and even more complicated molecules, namely an r^{-6} attraction at large distances and a steep repulsive wall at small distances. For the remainder of this section, the following reduced units will be used: reduced distance $r^* = r/\sigma$, reduced density $\rho^* = \rho\sigma^3$ and reduced temperature $T^* = kT/\epsilon$. The phase diagram of the Lennard-Jones systems, unlike that for the inverse-power potentials, is two-dimensional, that is, density and temperature are independent variables. This phase diagram has been mapped out by computer simulation.¹⁹ The crystal form of this material is face centered cubic (fcc). Some of the simulations listed here use a truncated or modified version of the Lennard-Jones potential. This makes comparison of the various simulations difficult since the phase diagrams of these altered potentials differ from that of the usual potential, especially in the triple point region where most simulations are performed.

The earliest attempt at a computer description of a Lennard-Jones interface used a static-hard-sphere computer-built model to estimate the interfacial free energy of a Lennard-Jones crystal/liquid system.³⁵ A computer-built model of a fcc (111) hard sphere crystal/liquid interface was constructed using the method of Zell and Mutaftschiev.³⁴ The vibrational properties and interfacial free energy were then estimated by assuming that the particles interacted via a Lennard-Jones potential. The structure was not allowed to relax from the hard-sphere configuration and exhibited the anomalous density deficiency at the interface that is a common feature of such static computer-built models.

The first *simulation* (as opposed to a model) of a LJ crystal/liquid interface was a three-phase study by Ladd and Woodcock,²⁶ whose primary purpose was to determine the LJ triple point, but which as a byproduct yielded a density profile of the fcc (100) interface. A molecular dynamics simulation of 1500 particles was performed in which the usual periodic boundary conditions in the z direction were replaced by static lattice on the crystal side and a hard wall bounding the vapor. The simulation gave a triple-point temperature of $T_{tp}^* = 0.72$ and crystal and liquid coexistence densities of 0.986 and 0.80, respectively. The (100) density profile is very broad, about $7-8\sigma$ ($9-10$ lattice spacings) wide. Unlike the hard sphere models, no density deficit was seen at the interface. Since only the top several layers are allowed to melt with the rest of the bulk crystal being static (effectively zero temperature), the relationship of this interface to a true equilibrium interface is difficult to evaluate. However, in this simulation the number of nonstatic crystal layers is great enough that the effect is probably small.

In a later paper,⁴⁵ Ladd and Woodcock expanded the analysis of their interface to include thermodynamic and transport properties. From a profile plot of the two-dimensional (layer) diffusion constant, the width of the interfacial region is estimated to be five lattice spacings with respect to particle transport, but the statistical error in this calculated quantity is rather large. The noise in a calculation of the surface stress was also too great to yield a reliable result.

Shortly after the Ladd and Woodcock simulation, the (100) fcc LJ interface was also simulated by Toxvaerd and Praestgaard⁴⁶ at a slightly higher reduced temperature of 1.15. The simulation box consisted of 1680 total particles with the liquid region sandwiched between two crystal slabs. Periodic boundary conditions were used in all three directions, so the crystal phase near the interface was allowed to fully relax without a zero-temperature boundary condition. The width of (100) interfacial region as estimated from the density profile was about $7-8$ lattice spacings, which was slightly narrower than that of the triple-point calculation of Ladd and Woodcock. This simulation together with the others mentioned earlier in this section have been also reviewed earlier.⁸

In a rather small ($N = 432$) simulation, Hiwatari, Stoll, and Schneider⁴⁷ have studied the (100) fcc crystal/liquid interface of a truncated Lennard-Jones system. Here the LJ potential is set to zero beyond the well minimum and shifted by ϵ to yield a purely repulsive potential. It should be noted that without an attractive well, this potential does not exhibit fluid/vapor coexistence and therefore a triple point cannot be defined. Molecular dynamics with fully periodic boundary conditions was used to simulate the interface with $\rho_c\sigma^3 = 1.12$, $\rho_l\sigma^3 = 0.97$. The coexistence temperature was found to be $kT/\epsilon \approx 0.20$. The analysis of the data focused on the layer-averaged potential energy (no density profile was calculated). The potential energy change through the interface from bulk crystal to bulk liquid behavior takes place over a rather narrow $3-4$ lattice, but the large statistical error due to the small size limits the usefulness of this result. Also the rather crude "trial and error" method used to determine the coexistence conditions for the truncated potential leaves much doubt as to whether equilibrium was ever properly established.

So far, all simulations concerned the (100) fcc interface orientation. Since the early hard-sphere-based static models, by construction, involved close-packed faces [fcc (111) or hcp (0001)], a full simulation study of these faces would help to evaluate the validity of such models. To this end, Bonissent, Gauthier, and Finney (BGF)⁴⁸ used the Monte Carlo method to simulate an hcp (0001) interface using 860 particles using a modified LJ potential

$$\phi_{\text{BGF}}(r) = \epsilon[(\sigma/r)^{12} - 2(\sigma/r)^6] \quad (17)$$

The energy and distance scales were arbitrarily chosen to approximate those of argon: $\epsilon = 1.7 \times 10^{-22}$ J and $\sigma = 3.76$ Å. The simulation temperature corresponded to 86 K ($kT/\epsilon = 0.70$) (slightly above the argon melting point of 83.8 K) with a crystal density of 2.50×10^{-2} Å⁻³ ($\rho\sigma^3 = 1.33$). The liquid density was not reported. Since the coexistence properties of this modified LJ potential are not known and no specific fitting seems to have been done, there is no guarantee that crystal/liquid equilibrium conditions can be reached with these parameters. Periodic boundary conditions were used only in the directions perpendicular to the interface. On the crystal side, only two of the six total crystal layers were allowed to move while the liquid region in contact with the crystal was 11σ wide and terminated in a free surface. The static hard-sphere crystal/liquid interface model of Mutaftschiev and Zell⁵ was used as the initial condition. As in the hard-sphere models, a density deficit was observed at the interface.

Later, Bushnell-Wye, Finney, and Bonissent⁴⁹ repeated the hcp (0001) calculation using the same potential, temperature and densities as BGF, but using a much larger system ($N = 4378$) with 10 movable crystal layers. In this larger calculation, no density deficit was seen, leading to the conclusion that it was an artifact of the use of a static crystal. Therefore, the static hard-sphere models and simulations in which only a few crystal layers are allowed to move severely underestimate the importance of the relaxation of the crystal phase in the formation of the equilibrium interface. It is difficult to compare this simulation and that of BFG with the other LJ simulations because of the difference in potential and the fact that the static crystal makes it difficult to assess the interfacial width.

The fcc (100) and (111) LJ interfaces were studied in detail by Broughton, Bonissent, and Abraham^{29,50} using molecular dynamics to simulate a system of 1764 atoms under LJ triple-point conditions. The density profiles for both faces were quite similar, with the crystal density oscillations decaying through the interface over a distance of about 6–8 lattice layers. Diffusion constant profiles for the two interfaces were calculated from the mean-squared xy (parallel to the interface) displacement in a given layer. These transport profiles are identical for both interfaces within the statistical noise and are about 3σ in width. This insensitivity of the diffusion constant to the interfacial orientation is consistent with that seen subsequently by Laird and Haymet²⁸ for the various bcc interfaces of the inverse sixth power potential. An attempt was made to estimate the interfacial free energy from the interfacial excess potential energy and an estimate of the entropy η from "free volume" considerations, but the large errors inherent in such a calculation made these estimates of limited value.

Landman, Barnett, Cleveland, and Rast⁵¹ performed a set of molecular dynamics simulations on an fcc crystal/liquid Lennard-Jones system in which the crystal is randomly doped with a 10% concentration of larger LJ impurity particles. The diameter and energy well depth ratios were chosen to correspond to an argon system with krypton impurities. In all, three interfaces were studied: (100), (110), and (111)—using 1500, 1505, and 1512 particles, respectively. The interfaces were created by melting the upper layers of a crystal slab and letting the resulting three-phase system come to equilibrium. The very lower layers of the slab were held static. The equilibrium temperature is claimed to be about 5% less than that expected for a pure argon system, although it is not quoted explicitly. Also not reported are the equilibrium crystal and liquid densities, making comparison with other simulations difficult. The quality of the density profiles is significantly poorer than that of other simulations reported here (especially for the (110) interface), but appear to give widths that range from 4–6 argon diameters (3.4 Å). The diffusion profile widths are about the same for all three interfaces, approximately four argon diameters. The system was analyzed as if it were a one-component system; no uniquely two-component quantities, such as excess particle densities, were measured. The reasons for the choice of this system are therefore not clear.

By far the most definitive set of interface simulations for the Lennard-Jones crystal/liquid system are those of Broughton and Gilmer. These studies of the struc-

ture⁵² and thermodynamics^{30,31} of fcc (100), (110), and (111) LJ crystal/liquid interfaces were part of an extensive six-part series on the bulk and surface properties of the LJ system. Like most of the earlier simulations, these were done under triple-point conditions. The numbers of particles for the (111), (100), and (110) simulations were 1790, 1598, and 1674, respectively. The relative amounts of crystal and liquid were approximately equal to one another for all studies. Analysis of $d = 2$ diffusion constants, various layer-dependent trajectory plots, pair-correlation functions, nearest neighbor fractions, and angular correlations yield a width of about three atomic diameters for all three interfaces. The density profiles appear to indicate an interface width that is larger than that predicted by the transport and local structure properties, a property also seen by Laird and Haymet²⁸ in the inverse sixth power system. This is interpreted to be due to large density oscillations present on the liquid side of the interface. Such oscillations can be induced by relatively small potential energy variations because of the large first peak in the liquid structure factor.

Broughton and Gilmer also attempt to measure the interfacial free energy for the three interfaces. Unlike the surface stress, which can be directly calculated from the pressure tensor, calculation of the interfacial free energy requires a much more complicated thermodynamic integration. Using a series of cleaving potentials (see section III for details), Broughton and Gilmer calculate the reversible work necessary to form the interface in a four-step process. The first two steps involve the cleaving of the bulk crystal and bulk liquids into two parts. In the third step, the cleaved crystal and liquid are brought together and finally the cleaving potentials are slowly reduced until the crystal and liquid are in equilibrium contact. Summing the total integrated reversible work for these four steps yields the γ_{cl} for the interface in question. The calculated interfacial free energies were shown to be only weakly dependent upon the interfacial orientation. The resulting values are 0.35 ± 0.02 , 0.34 ± 0.02 and 0.36 ± 0.02 in units of ϵ/σ^2 for the (111), (100), and (110) interfaces, respectively.

To test the effect of system size on interfacial simulations, Galejs, Raveché, and Lie⁵³ studied the LJ fcc (100) and (111) crystal/liquid interface with molecular dynamics on systems of approximately 35 000 particles at a reduced temperature of 1.15 and crystal and liquid coexistence densities of 1.024 and 0.936, respectively. These conditions are nearly identical to the earlier LJ fcc (100) simulation of Toxvaerd and Praestgaard.⁴⁶ After equilibration the (100) and (111) interface systems were run for 12 800 and 13 500 time steps, respectively ($\delta t = 0.0046(m\sigma^2/\epsilon)^{1/2}$ or 10 fs when parameters corresponding to argon are used). The density profiles have widths of about seven lattice spacings for both interfaces, which corresponds to 5σ for (100) and 6σ for (111). The (100) density profile width calculated here is identical to that for an earlier, smaller ($N = 1680$) simulation⁴⁶ on this system, indicating that—except for improved statistics—there are no appreciable size effects. Individual layer profiles of the potential energy are also calculated and give interface widths of about 5σ for both interfaces. Since the potential energy profile is a better indication of the local environment than is the density profile, this data

supports the observations in earlier simulations that the interfacial width is generally independent of interfacial orientation. Analysis of contour plots for various lattice order parameters was interpreted to indicate that each interfacial layer actually consisted of islands of "crystallike" and "liquidlike" particles, contradicting the analysis of Tallon.⁴¹

V. Results for More Complex Systems

A. The Ice/Water Interface

Water plays a unique role as a solvent, and the behavior of water near an interface is important for the microscopic study of macromolecules and polyelectrolytes,⁵⁴ leading to a better understanding of interfaces between aqueous solutions and biomembranes⁵⁵ and electrodes.⁵⁶ In a series of simulations, the crystal/melt interface for two different models of water have been investigated. First, Karim and Haymet^{57,58} studied the interface using the TIP4P^{59,60} model water interactions. In order to determine the extent of model dependence in the results, Karim, Kay, and Haymet⁶¹ later repeated these calculations using the SPC⁶² water model. These studies represent the first attempts to simulate the interface between a molecular fluid and its crystal and have special significance because angular dependent forces were included in the interfacial simulation.

The structure of ice 1h has been studied intensely by experimental methods such as X-ray and neutron scattering, as well as NMR and laser spectroscopy.⁶³ Ice 1h is known to be one of the most thoroughly disordered crystalline substances. In addition to the prevailing oxygen disorder, the hydrogen atoms are also known to be disordered. On the basis of entropy arguments, the molecules in ice are known to obey the so-called "ice rules". Karim and Haymet chose to study an ordered ice 1h structure, since this offers a tractable starting point for theoretical investigations. The structure of bulk water has also been extensively studied by experimental methods.^{64,65}

Recent experimental studies of the vapor/solution interface with aqueous solutions⁶⁶⁻⁶⁸ have been able to probe the orientational order of the molecules in the interfacial region using second harmonic generation (SHG) methods. More recently, SHG optical scattering techniques have been used to probe the structure of vapor/water interface.¹⁴ These methods indicate that near the interface, on the liquid side, the water dipole is oriented toward the liquid.

The ice/water interface can also be studied by methods applied to the water/vapor interfaces. However, to date no experiments have been published that probe the equilibrium structure of the ice/water interface. Most experiments on the ice/water interface have focused on the growing interface,⁶⁹⁻⁷² using light scattering or ellipsometry. However, the structure revealed by these experiments has been on the scale of hundreds of angstroms, and is probably due to the concentration gradient of impurities forced in front of the growing interface. In addition, it is likely that a nonequilibrium interface is much broader than an equilibrium one. Experiments with better length resolution are needed to probe the structure of the equilibrium ice/water interface.

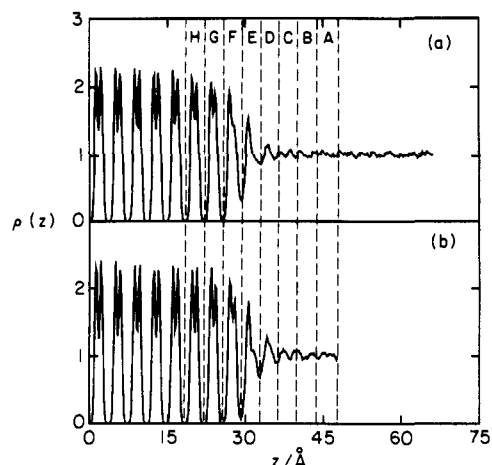


Figure 10. The oxygen density profile for the folded TIP4P water interface: (a) results obtained from the larger simulation; (b) the results obtained from the previous, smaller simulation (ref 58). The layers A through H are demarcated by the dashed lines. (Reprinted from ref 58. Copyright 1988 American Institute of Physics.)

The original ice/water interface simulations used the TIP4P^{59,60} model for water. This is a rigid, 4-center model which gives good thermodynamic and structural properties for bulk water, over a wide range of temperatures and pressures. In the TIP4P model, there are three charges on the water molecule: two of magnitude $+q$ located on each of the hydrogen atoms, and one of magnitude $-2q$ on a site M located on the HOH bisector but not at the location of the oxygen atom. There is also a Lennard-Jones interaction between each oxygen site. These Coulomb and Lennard-Jones potentials are, respectively, as follows:

$$\Phi_{\text{Coul}} = \sum_{\text{sites } i < j} \frac{q_i q_j}{r_{ij}} \quad (18)$$

$$\Phi_{\text{LJ}} = \sum_{i < j} \left[\frac{A^2}{r_{ij}^{12}} - \frac{C^2}{r_{ij}^6} \right] \quad (19)$$

where q_i and q_j refer to charges on different molecules and A and C are the Lennard-Jones (LJ) parameters for this model. The values of the parameters are tabulated in ref 58. In the simulations, the pair interactions are switched off smoothly between 8.1 Å and 8.5 Å. At and beyond 8.5 Å the potential and force are both set to zero.

The MD simulations were performed in the NVE ensemble using the Verlet algorithm with SHAKE⁷³ to integrate the equations of motion for each molecule. The time step used during equilibration and averaging was 6 fs. For the calculations an antiferromagnetic (AF) structure of ice 1h was chosen. This structure has a net dipole moment of zero.

The structure and thermodynamics of TIP4P ice are not known. For the purpose of this study, an exhaustive study of possible TIP4P ice 1h structures was not performed. Haymet and Karim were able to obtain ice 1h at a reasonable temperature and pressure, which was stable on the time scale of 100 ps without structural breakdown, and hence a stable ice/water interface under physical conditions reasonably close to experiment. The TIP4P model can be considered a good starting point for the study of the ice/water interface.

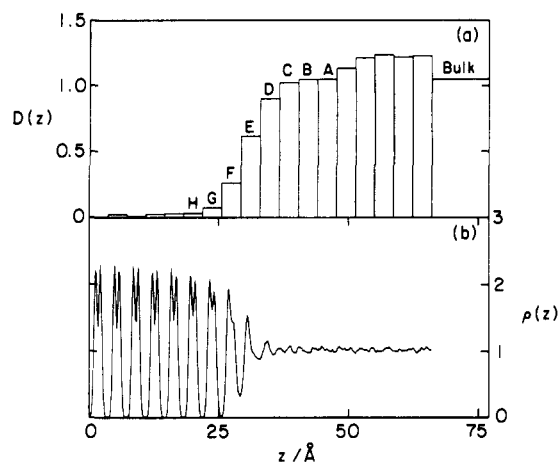


Figure 11. The diffusion constant (D) across the TIP4P water interface: (a) histogram of values in units of $10^{-5} \text{ cm}^2/\text{s}$; (b) the density profile reproduced from the Figure 10. (Reprinted from ref 58. Copyright 1988 American Institute of Physics.)

In order to construct the ice/water interface, separate, equilibrated samples of ice 1h and bulk water were obtained. The ice was prepared from a unit cell with eight TIP4P water molecules in an antiferromagnetic structure. The coordinate axes were chosen such that the z axis corresponds to the crystallographic c axis. The molecules were oriented with the O–H bonds placed symmetrically about the O–O directions, since the H–O–H angle for the TIP4P molecule is not precisely the tetrahedral angle. The temperature profile of the system was also observed to be uniform. The dimensions of the simulation box were $46.5 \times 35.8 \times 146.9 \text{ \AA}$. This system was equilibrated for 30 ps and averages taken over a further 48 ps. The average density profile is shown in Figure 10. Comparison of this density profile to that of an earlier smaller simulation⁵⁷ indicates that the density profile is independent of system size.

The diffusion constant across the interface provides a different, but equally valid, measure of the extent to which the interfacial structure is crystallike or liquidlike. The diffusion constant is calculated from the measured average mean square displacement (MSD) as a function of time for various layers through the interface. The oxygen center is used to label the position of a molecule. There are approximately 200 molecules per layer, and each molecule is identified with a given layer for 2.4 ps. A histogram of the diffusion constant profile is shown in Figure 11 together with the value of the diffusion constant calculated from a separate simulation on a bulk sample of 288 molecules with density 1.02 g/cm^3 . This bulk diffusion constant is somewhat smaller than the value in the layers of the liquid farthest from the interface, possibly due to the fact that the density of the layers in the interface simulation is not fixed precisely at 1.02 g/cm^3 .

To determine if the structure within individual interface layers is homogeneous or if patches of localized (crystallike) and free (liquidlike) molecules exist in a given layer, continually restructuring dynamically with the time evolution of the system, the following analysis was performed. Dynamical trajectories of molecules in the different layers through the interface were calculated. At a fixed time ($t = 0$), each molecule is assigned to a layer, depending on its z coordinate. This molecule is then identified with that layer for the remainder of this trajectory analysis. The molecular

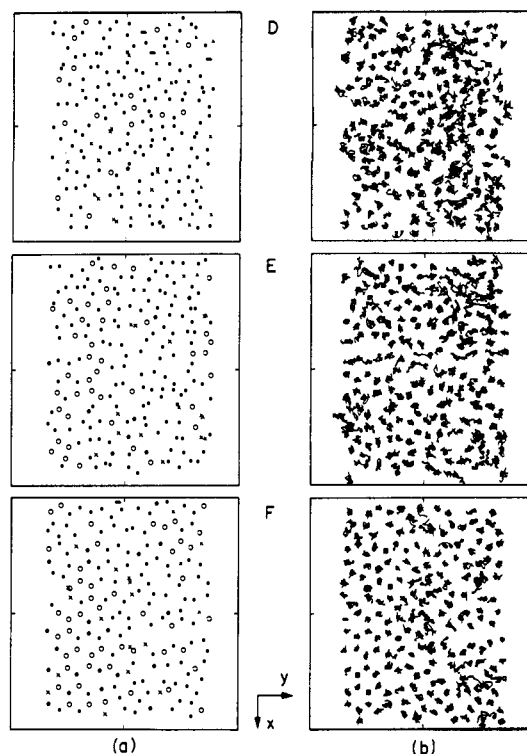


Figure 12. Oxygen atom trajectories projected on to the TIP4P water interfacial (xy) plane for the layers D, E, and F: (a) mean position of oxygen atoms are marked by an "x" or an "o" according to the criteria defined in the text; (b) actual trajectories of oxygen atoms. (Reprinted from ref 58. Copyright 1988 American Institute of Physics.)

trajectories are then recorded for 6.6 ps, and the positions of the oxygen atoms noted every 0.12 ps. From these recorded configurations, the mean position of the molecules can be calculated. These trajectories are plotted in Figure 12b for layers D, E, and F. It is immediately apparent that layer D has disorder characteristic of a liquid. Layer E shows some evidence of order, while layer F has large regions of order characteristic of the crystal. For easier representation of the trajectories, the actual plots have been simplified in Figure 12a. Here the mean positions of the oxygen atoms are plotted. Those atoms with total displacement from the initial position less than 1.58 \AA and that are within a distance 1.1 \AA of an ideal lattice site are denoted by an "o". All other molecules are denoted by an "x". These plots display the hexagonal ordering in layer F characteristic of the ice lattice, and the disorder in layer D characteristic of the liquid.

In addition to the density profile and the diffusion constants, the time-averaged one-body orientational correlation functions of the water molecules were also measured. The polar orientation angle θ and ϕ were measured for both the dipole direction vector and the H–H direction vector, defined in Figure 13, parts a and b, respectively. For the dipole unit vector, the quantities

$$P_D(\theta) d\theta = \langle \theta \rangle_\phi d\theta \quad 0 < \theta < \pi \quad (20)$$

and

$$P_D(\phi) d\phi = \langle \phi \rangle_\theta d\phi \quad 0 < \phi < \pi \quad (21)$$

were calculated.

Thus, the angle θ is averaged over all ϕ , and ϕ is averaged over all θ . For a pure liquid with random orientation of the vectors

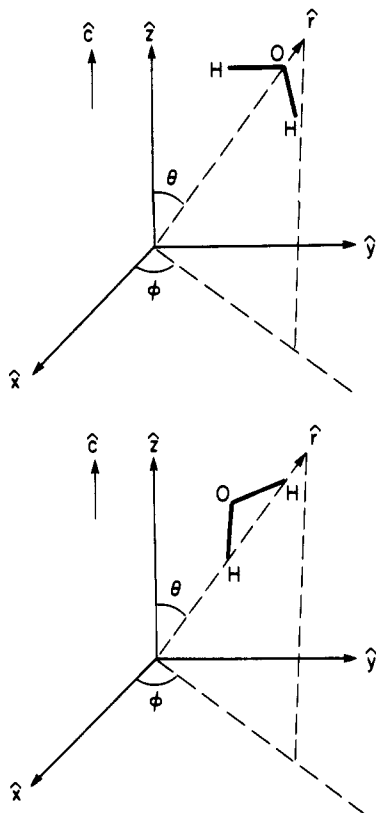


Figure 13. The definition of the angles θ and ϕ (a) for the water molecule dipole moment vector and (b) for the intramolecular hydrogen-hydrogen vector. The location of oxygen and hydrogen atoms are labeled by O and H, respectively. The crystallographic c axis is indicated. (Reprinted from ref 58. Copyright 1988 American Institute of Physics.)

$$P_D(\theta) = \frac{1}{2} \sin \theta \quad (22)$$

and

$$P_D(\phi) = \frac{1}{2\pi} \quad (23)$$

For the H-H direction vector, the definitions for $P_H(\theta)$ and $P_H(\phi)$ are identical to those in eqs 22 and 23 above. These orientational correlation functions are plotted in Figures 14-17. In order to smooth the noisy data, each point is replaced by the average over the five neighboring points on each side. Thus each point represents an average over 11 degrees.

For the dipole quantity $P_D(\theta)$, layer F has the twin-peaked structure characteristic of the crystal. Layer E has intermediate structure whose origin is now clear from the above description of the trajectories. Layer D contains some of the orientational order characteristic of the ice lattice. This layer has translational properties indistinguishable from that of the bulk liquid but includes some orientational structure of the ice lattice. Layer C and G are identical to the correlation expected from a pure liquid and a pure crystal, respectively. Similar analysis applies to the $P_D(\phi)$ and $P_H(\theta)$ correlations. However, $P_H(\phi)$ shows structure extending into layer C also. Thus the presence of the crystal influences the liquid correlations as far away as layer C. Hence, the orientational order induced by the ice crystal propagates at least one, and possibly two layers deeper into the water than translational order. This could be an extremely important effect in electrochemical sys-

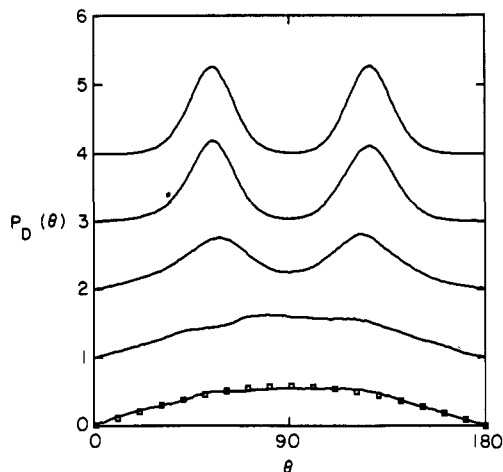


Figure 14. The probability correlation $P_D(\theta)$ of the TIP4P water dipole angle, defined by eq 20. From top to bottom, the curves correspond to layers G, F, E, D, and C. The squares are the points given by eq 22. (Reprinted from ref 58. Copyright 1988 American Institute of Physics.)

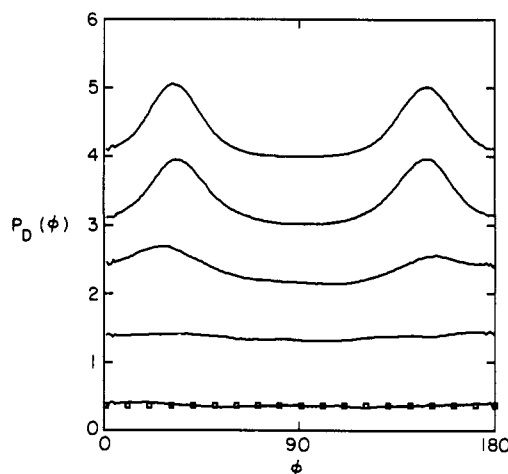


Figure 15. The relative probability $P_D(\phi)$ of the TIP4P water dipole angle, defined by eq 21. From top to bottom, the curves correspond to layers G, F, E, D, and C. The squares are the points defined by eq 23. (Reprinted from ref 58. Copyright 1988 American Institute of Physics.)

tems and biological membranes, and will be studied further. In all cases symmetry about $\theta = \pi/2$ is observed, indicating no symmetry breaking orientations through the interface. This is distinct from the case observed in simulations on the liquid/vapor interface.⁷⁴

In summary, on the length scale investigated here, size effects do not play a role in the structure of the interface, which is unchanged from the result obtained for a smaller system. There are definite regions in the simulation box corresponding to bulk liquid, bulk crystal and the interface. The interface is found to be stable for at least 100 ps and is found to be 10-15 Å wide.

In a latter work, Karim, Kay, and Haymet⁸¹ repeated the ice/water simulations using the simple point-charge model of water⁶² to study possible model dependence of the measured interfacial properties. Apart from the further decrease in the apparent bulk melting temperature from 240 to 200 K, there is no significant difference. This constitutes evidence that the measured properties are reasonably independent of the particular model of water and plausibly represent the actual properties of the real ice/water interface.

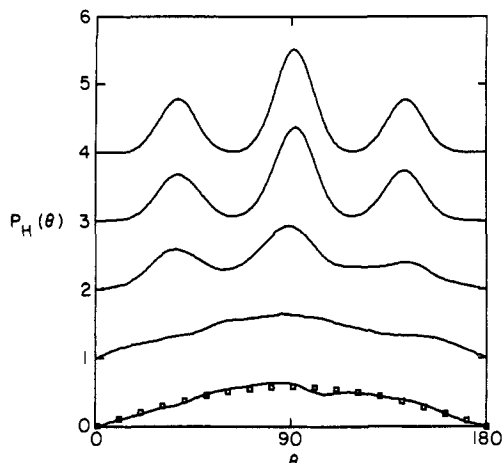


Figure 16. The relative probability $P_H(\theta)$ of TIP4P water H-H angle, defined similar to eq 20. From top to bottom, the curves correspond to layers G, F, E, D, and C. The squares are the points given by the equation corresponding to eq 22. (Reprinted by permission from ref 58. Copyright 1988 American Institute of Physics.)

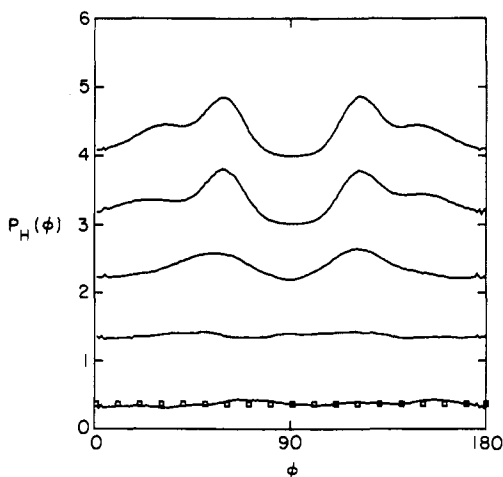


Figure 17. The relative probability $P_H(\phi)$ of the TIP4P water H-H angle, defined similar to eq 21. From top to bottom, the curves correspond to layers G, F, E, D, and C. The squares are the points defined given by the equation corresponding to eq 23. (Reprinted from ref 58. Copyright 1988 American Institute of Physics.)

B. The Silicon Interface

Crystalline silicon, one of the technologically most important of materials, is prepared primarily via growth from the melt. Therefore, given the close connection between such crystal growth and the equilibrium interfacial structure and dynamics, the silicon crystal/liquid interface is a prime candidate for study using computer simulation.

Within the bounds of a classical simulation, silicon cannot be described by a simple pairwise additive interaction potential alone, due to the directional nature of its covalent bonding. To describe correctly the tendency toward tetrahedral bonding requires specification of three-body (or higher) contributions to the interaction energy. Using properties of crystal and liquid silicon in the vicinity of the melting point, Stillinger and Weber (SW)⁷⁵ devised a potential that is successful in predicting the bulk liquid and crystal properties when simulated. This potential consists of a two-body interaction that features a short-ranged repulsion and an attractive well:

$$\begin{aligned} \phi_2(r) &= A(\text{Br}^{-4} - 1) \exp[1/(r - a)] & r < a \\ &= 0 & r > a \end{aligned} \quad (24)$$

A three-body term designed to account for the covalent bonding was also included

$$\phi_3(\mathbf{r}_i, \mathbf{r}_j, \mathbf{r}_k) = h(r_{ij}, r_{ik}, \theta_{jik}) + h(r_{ij}, r_{jk}, \theta_{ijk}) + h(r_{ik}, r_{kj}, \theta_{ikj}) \quad (25)$$

where

$$h(r_{ij}, r_{ik}, \theta_{jik}) = \lambda \exp\left[\frac{\gamma}{r_{ij} - a} + \frac{\gamma}{r_{ik} - a}\right] (\cos \theta_{jik} + 1/3)^2 \quad (26)$$

and θ_{jik} is the angle formed by atoms j , i , and k . With distance r expressed in units of 2.0951 Å and energy in units of 50 kcal/mol, the parameters optimized by SW are

$$A = 7.049\ 556\ 277 \quad (27)$$

$$B = 0.602\ 224\ 5584 \quad a = 1.8 \quad \lambda = 21.0 \quad \gamma = 1.20 \quad (28)$$

The $1/3$ in the angular-dependent part of three-body potential ensures that the tetrahedral geometry is favored. This potential predicts correctly that the lowest energy crystal structure is a fcc diamond lattice.

Using the SW potential, Abraham and Broughton²⁷ simulated the (111) and (100) silicon crystal/melt interface under three-phase coexistence (triple-point) conditions. Using an estimate of 1760 K for the triple-point temperature of SW silicon, the two interfaces were studied in separate molecular dynamics simulations of approximately 1800 atoms each. Each simulation box contained three phases ordered along the z axis: crystal, liquid, and vapor. Periodic boundary conditions in all three coordinate directions gives a simulation with three different interfaces: crystal/liquid, crystal/vapor, and liquid/vapor. The system was equilibrated for 20 000 time steps ($\delta t = 3.8 \times 10^{-16}$ s).

The shift in the local environment from tetrahedral bonding in the crystal to the higher coordination numbers present in the liquid is best illustrated by individual layer profiles of the three-body energy density. For a perfect crystal the contribution of the three-body potential vanishes because each silicon atom has a tetrahedral environment in the diamond lattice. The higher coordination number (about 8) of the atomic environment in the liquid phase raises the three-body energy considerably, but this effect is compensated by a lowering of the two-body energy by bringing more atoms into the attractive two-body energy well around a given central atom.

Figure 18 shows the number density profile and three-body potential energy profile for the (111) and (100) silicon interface simulations. The profiles indicate that the (111) crystal/liquid interface is relatively sharp (about 3 reduced length units or 6 Å wide) and that the (100) interface is somewhat broader with a width of about 8 Å.

Landman et al.⁷⁶ also used the Stillinger-Weber potential to simulate the Silicon (100) and (111) crystal/melt interfaces. The interfaces were created by melting the top half of a crystal slab by a local temperature increase. Periodic boundary conditions were employed only in the x and y directions (parallel to the interface). The deepest inner layers of the crystal

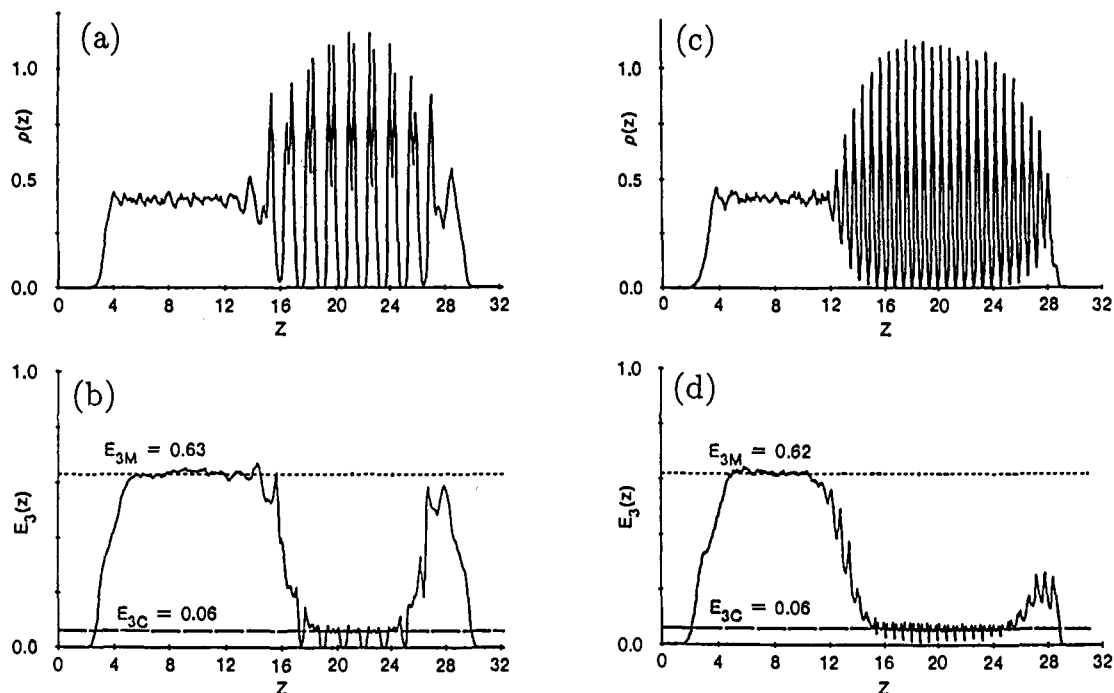


Figure 18. (a) Equilibrium number density, (b) three-body potential energy density profiles for the (111) interface, (c) equilibrium number density, and (d) three-body potential energy density profiles for (100) interface for the triple-point silicon system. (Reprinted from ref 27. Copyright 1986 American Institute of Physics.)

were kept fixed and the z direction length was such as to allow a region of vapor (vacuum) beyond the liquid phase. For the (100) interface, two system sizes were studied: 28×36 and 24 layers \times 144 particles per layer, respectively. For the (111) interface a system that is 20×49 was used. Equilibration for about 150 000 time steps (about 60 ps) gives a melting temperature of about 1665 K (the experimental melting temperature is 1683 K). As seen by Abraham and Broughton, the (111) interface is relatively sharp. The (100) interface is broader and a side view of the interface showed that this interface was made up of alternating (111) and $(\bar{1}\bar{1}\bar{1})$ facets in a zigzag pattern. Landman et al. also see similar faceting in experiments on real silicon interfaces performed in situ. The size of the facets in the experiments ($3 \mu\text{m}$) are much larger than those seen in the simulations that are only a few angstroms across. The size disparity indicates that this is not an equilibrium phenomenon but a kinetic one; that is, a (111) interface melts more slowly than a (100) one.

VI. Theory of the Crystal/Liquid Interface

Early theories of crystal/liquid interfaces were based on phenomenological models of interface structure that were extensions of models perhaps more suited to other types of interfaces. At one end are models such as that due to Jackson⁷⁷ that view the interface as being relatively sharp with a clear distinction between "liquid" and "crystal" particles even at the interface. At the other are theories of diffuse structureless interfaces⁷⁸ that, while useful for liquid/vapor interfaces, are not ideal for the highly structured crystal/liquid case.

To date, the only microscopic theories that are well suited to calculate both the detailed structure and thermodynamics of a crystal/liquid interface are those based on various forms of density functional (DF) theory, which is a procedure for determining the free energy associated with a given spatially dependent

single-particle density, $\rho(\mathbf{r})$. That is, the free energy is determined as a *functional* of $\rho(\mathbf{r})$. The equilibrium free energy and microscopic density can then be found by minimizing this functional over the space of single-particle densities consistent with the ensemble under study. A detailed description of basic classical DF theory and its mathematical justifications is presented by Evans.⁷⁹ Note that there is no existing DF theory for the diffusion profile.

Since coexisting crystal and liquid phases have different bulk densities in general, a DF theory for the crystal/liquid interface is best constructed within a grand canonical ensemble framework. According to Mermin,⁸⁰ for a system at fixed temperature, T , chemical potential, μ , and external single-particle potential, $v(\mathbf{r})$ there exists a functional $\mathcal{F}[\rho(\mathbf{r})]$, independent of $v(\mathbf{r})$ and μ , such that the functional

$$\Omega[\rho(\mathbf{r})] = \mathcal{F}[\rho(\mathbf{r})] + \int d\mathbf{r} [v(\mathbf{r}) - \mu] \quad (29)$$

is a minimum for the correct equilibrium density $\rho(\mathbf{r})$ subject to the external potential. The value of Ω at this minimum is the value of the grand potential. (For systems restricted to constant density, i.e. canonical ensemble, one minimizes the functional \mathcal{F} itself to give the equilibrium Helmholtz potential.)

The functional $\mathcal{F}[\rho]$ can be written as the sum of an ideal part, $\mathcal{F}_{\text{id}}[\rho]$, and an excess part, $\mathcal{F}_{\text{ex}}[\rho]$, due to the interparticle interactions:

$$\mathcal{F}[\rho] = \mathcal{F}_{\text{id}}[\rho] + \mathcal{F}_{\text{ex}}[\rho] \quad (30)$$

The ideal part is known exactly, and for a monatomic system is given by

$$\mathcal{F}_{\text{id}}[\rho] = \int d\mathbf{r} \rho(\mathbf{r}) [\ln[\Lambda^3 \rho(\mathbf{r})] - 1] \quad (31)$$

where Λ is the thermal wavelength. The excess part is, in general, unknown; therefore, the central task of a DF theory is to provide a suitable approximation for this quantity.

Density functional theories begin by defining the n -body direct correlation functions, $c^{(n)}(\mathbf{r}_1, \dots, \mathbf{r}_n; [\rho])$, in terms of the functional derivatives of $\mathcal{F}_{\text{ex}}[\rho]$:

$$c^{(n)}(\mathbf{r}_1, \dots, \mathbf{r}_n; [\rho]) = - \frac{\delta^{(n)} \beta \mathcal{F}_{\text{ex}}[\rho]}{\delta \rho(\mathbf{r}_1) \dots \delta \rho(\mathbf{r}_n)} \quad (32)$$

For arbitrary $\rho(\mathbf{r})$, the correlation functions, like $\mathcal{F}[\rho]$ itself, are unknown, except in the homogeneous density (liquid) limit, where, due to the advances in liquid state theory over the past three decades, they can be determined for $n \leq 2$. Density functional theories crystal/liquid phase coexistence exploit this knowledge of the liquid correlation functions to try and obtain approximations for those in an inhomogeneous phase.

Before the calculation of the interfacial properties can proceed, the density functional theory must be used to determine the equilibrium freezing properties of the system at the required temperature. The structure and thermodynamics of the coexisting liquid and crystal phases are needed to determine the boundary conditions of the density profiles on either side of the interface. The equilibrium freezing calculation may be summarized as follows. First, the periodic single-particle density of the crystal is parametrized so that the minimization of the free-energy functional can be performed. The most general parametrization for a given lattice type is the Fourier series

$$\rho(\mathbf{r}) = \rho_l [1 + \eta + \sum_{\{\mathbf{k}\}} \mu(\mathbf{k}) e^{i\mathbf{k} \cdot \mathbf{r}}] \quad (33)$$

where ρ_l is the bulk liquid density, η is the fractional density change on freezing, \mathbf{k} represents the set of reciprocal lattice vectors (RLV's) corresponding to the particular lattice type under study, and $\rho_l \mu(\mathbf{k})$ is the Fourier component of the density corresponding to the wavevector \mathbf{k} . A simpler, but less general, parametrization that is commonly used expresses the density as a sum of Gaussian peaks centered at the lattice sites

$$\rho(\mathbf{r}) = (\alpha/\pi)^{3/2} \sum_i \exp(-\alpha|\mathbf{r} - \mathbf{R}_i|^2) \quad (34)$$

where the \mathbf{R}_i are the real space lattice vectors and α measures the width of the Gaussian peaks. For fcc systems, the Gaussian parametrization has been found to give almost identical freezing results as the more complicated, but more general Fourier expansion.⁸¹ After parametrization of the crystal density, the free energy (grand or Helmholtz) is minimized in such a way as to ensure the thermodynamic conditions of phase coexistence are satisfied, that is, the pressure, temperature, and chemical potential of the crystal phase equals that of the liquid phase. The $\rho(r)$ at the minimum is the equilibrium crystal density. (For further information about this aspect of the calculation, there are several reviews in the literature.⁸²⁻⁸⁴)

Once the equilibrium phases have been determined, a parametrization of the interfacial $\rho(\mathbf{r})$ is constructed by allowing the order parameters used in the equilibrium calculation to vary with z , the coordinate perpendicular to the interface. The shape of these z -dependent order parameter profiles, as well as the interfacial excess free energy, can then be determined from the minimization condition, together with the boundary conditions [the order parameters must tend toward their crystal (liquid) equilibrium values as z goes to $+\infty$ ($-\infty$)]. Many authors also assume that the

Fourier components vary slowly across the interface allowing a square-gradient approximation to be used.

The first attempt to apply the density functional formalism to the problem of the crystal/liquid interface was the work of Haymet and Oxtoby (HO).⁸⁵ Their approach was based on an earlier theory of freezing due to Ramakrishnan and Yussouff⁸⁶ that HO generalized to a nonlinear theory and reformulated into the language of classical density functionals. In this theory, the free energy of the inhomogeneous phase (here, the crystal) is expanded in a functional Taylor expansion about a reference liquid density. This expansion is subsequently truncated at second order to yield

$$\begin{aligned} \beta \mathcal{F}_{\text{ex}}[\rho] = & \beta \mathcal{F}_{\text{ex}}(\hat{\rho}) - c_1^{(1)}(\hat{\rho}) \int d\mathbf{r}_1 [\rho(\mathbf{r}_1) - \hat{\rho}] - \\ & \frac{1}{2} \int \int d\mathbf{r}_1 d\mathbf{r}_2 c_1^{(2)}(|\mathbf{r}_1 - \mathbf{r}_2|; \hat{\rho}) [\rho(\mathbf{r}_1) - \hat{\rho}] [\rho(\mathbf{r}_2) - \hat{\rho}] + \dots \end{aligned} \quad (35)$$

In the HO formulation, the reference density is chosen to be that of the equilibrium liquid.

The Fourier parametrization, used in the original paper by Haymet and Oxtoby,⁸⁵ is more general than the Gaussian, but is more complex. In practical calculations, the expansion for $\rho(\mathbf{r})$ must be truncated after the first few Fourier components. Hence, Haymet and Oxtoby chose the bcc/melt interface to study because, unlike the fcc system (which at that time was the only crystal/melt system studied by simulation), it is possible to find physically reasonable solutions to the equilibrium freezing problem for a small number of Fourier order parameters. (Unfortunately, subsequent calculations have shown that these bcc solutions are no longer obtained when a higher level theory with more Fourier order parameters is considered.) This very simple level of density functional theory predicts the 10–90 width of the fractional density change η for both the bcc (100) and (111) interfaces (the (110) was not studied) to be approximately given by

$$l_{10-90} \approx 3.7[-c''(k_1)]^{1/2} \quad (36)$$

where $c''(k_1)$ is the second derivative of the liquid two-particle direct correlation function evaluated at the magnitude of the nearest neighbor RLV of the crystal. For the inverse sixth power potential bulk liquid at $\rho_l^* = 0.6833$ and $T^* = 0.1$, $c''(k_1)$ was measured in a simulation of 432 particles to be about $-1.17\sigma^3$. This leads to a 10–90 width of about 4.1σ or 6 and 10 lattice planes for the (100) and (111) interfaces, respectively. Defining μ_1 to be the Fourier component of those nearest neighbor reciprocal lattice vectors at a 45° angle to the interfacial plane, the splitting of the $\eta(z)$ and $\mu_1(z)$ profiles, as described by Haymet and Oxtoby,⁸⁵ leads to a interfacial peak height that would be slightly broader than this η profile, but by only at most a few tenths of σ . Hence, this theory leads to interface widths that are similar to, but slightly smaller than, the widths measured in simulations of Laird and Haymet.²⁸

Recent work on the density functional theory of crystal/liquid interfaces has focused on the less complex Gaussian parametrization, which in principle provides a better representation of the bulk crystal freezing than a severely truncated Fourier expansion (but still less accurate than a full Fourier expansion). Moore and Raveché⁸⁷ make the ansatz that the single particle density of the interfacial system can be written

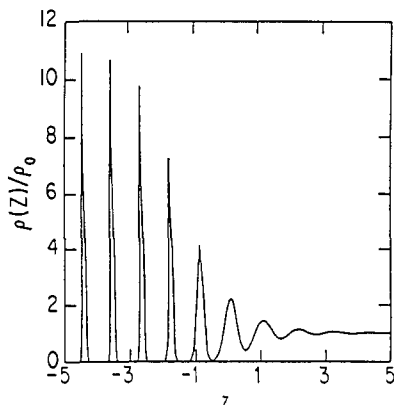


Figure 19. Theoretical density profile for the (111) hard-sphere interface as calculated by Oxtoby and McMullen using a four-parameter Gaussian density parametrization. (Reprinted from ref 89. Copyright 1988 Gordon and Breach Science Publishers, Inc.)

$$\rho(\mathbf{r}) = \rho_l + f(z)[\rho_s(\mathbf{r}) - \rho_l] \quad (37)$$

where ρ_l is the bulk liquid density, $\rho_s(\mathbf{r})$ is the bulk, spatially varying crystal density (given by eq 34), and $f(z)$ is a switching function that goes from 0 to 1 as the interface is traversed from the bulk liquid to the bulk crystal. They then minimize a second-order Helmholtz free energy functional (also using a square-gradient approximation) using a hyperbolic tangent parametrization of $f(z)$ to obtain the interfacial properties. Application of their theory to the fcc (100) and (111) Lennard-Jones interfaces gives results that are very sensitive to the input parameters. The resulting range of results for a reasonable spread of input values does overlap with the simulations on this system, but is rather large, making comparison difficult. However, comparison of the theoretical results for the interfacial width and free energy for the two interfaces studied, (100) and (111), for a given realization of the input parameters indicates a very strong dependence on the interfacial orientation, in direct contradiction to the simulation results.

McMullen and Oxtoby^{88,89} have taken a significant additional step by allowing the Gaussian width parameter α to vary with z . The form of this variation is determined by making the ansatz that the zero magnitude (bulk density) and first non-zero magnitude RLV Fourier components of $\rho(\mathbf{r})$ have shifted hyperbolic tangent profiles. This gives a four-parameter form (representing the widths and centers of the two profiles) for the single-particle density. Minimizing the same grand potential functional used by Haymet and Oxtoby, without invoking the square-gradient approximation, McMullen and Oxtoby examine the hard-sphere interfaces. The predicted interfacial free energies for the (100), (110), and (111) interfaces are nearly identical with an upper bound of $1.7kT/\sigma^2$. Using a slightly different ansatz in which relaxation of the spheres away from the bulk crystal lattice sites is allowed only in the direction perpendicular to the interface (z direction), Oxtoby and McMullen⁸⁹ obtained an upper bound on γ_{cl} of $4.0kT/\sigma^2$, showing a sensitivity of the results on the specific parametrization used. Figure 19 shows the results using the second ansatz for the density profile of the (111) interface. Although no hard-sphere crystal/melt interface simulations have been performed to make a direct comparison possible, the interfacial structure they obtain does compare very favorably with existing simulations of the Lennard-Jones interface.

Using a similar second-order functional, Mikheev and Trayanov⁹⁰ studied the fcc (111) crystal/liquid interface of a hard-sphere system using a Gaussian density parametrization for the crystal phase. The decay of the crystal peaks across the interface into the liquid phase is described by two order parameters governing the decay of the Fourier components of the Gaussians perpendicular and parallel to the interface, respectively. Minimizing the free energy yields the result that the ordering perpendicular to the interface decays at a slower rate than that for the density oscillations parallel to the interface, which have a relatively sharp density profile. Again, the results cannot be directly compared to simulation, but they are consistent with the existing Lennard-Jones calculations.

The hard-sphere crystal/liquid interface has also been studied by Curtin,^{91,92} who minimized a grand potential functional derived using a weighted density functional formalism.⁹³ Initiated by Tarazona,⁹⁴ this weighted density functional method is a modification of the usual Local Density Approximation (LDA) for inhomogeneous systems. In the LDA, the free energy density at a point \mathbf{r} in a system with inhomogeneous single-particle density $\rho(\mathbf{r})$ is given by the free energy of a homogeneous system, evaluated at the value of the single-particle density at point \mathbf{r} . However, for very strongly inhomogeneous systems such as a crystal, the LDA breaks down. To remedy this, the local density is averaged over a small region using a weighting function $w(|\mathbf{r}_1 - \mathbf{r}_2|; \hat{\rho})$ to create a coarse-grained or "weighted" density $\hat{\rho}(\mathbf{r})$:

$$\hat{\rho}(\mathbf{r}_1) = \int d\mathbf{r}_2 \rho(\mathbf{r}_2) w[|\mathbf{r}_1 - \mathbf{r}_2|; \hat{\rho}(\mathbf{r}_1)] \quad (38)$$

The local density approximation is then applied to this weighted density; that is, the free energy functional is given by

$$\beta\mathcal{F}[\rho] = \int d\mathbf{r} \beta f_0[\hat{\rho}(\mathbf{r})] \rho(\mathbf{r}) \quad (39)$$

where $f_0(\rho)$ is the excess Helmholtz free energy per particle of a homogeneous system of density ρ . The task of a successful weighted density functional theory is to choose a weighting function that leads to a good description of the structure and thermodynamics of the inhomogeneous phase.

In the weighted density approximation (WDA) of Curtin and Ashcroft,⁹³ the weighting function $w(|\mathbf{r}_1 - \mathbf{r}_2|; \hat{\rho})$ is chosen such that both the free energy and the two-particle direct correlation function $c^{(2)}$ (as defined in eq 36) are exactly reproduced in the limit of a homogeneous density. This requirement leads to a differential equation for the weighting function. The resulting functional gives very good results when applied to the problem of hard-sphere freezing. Using the WDA and a Gaussian two-parameter fit for the single-particle density through the interface similar to that of McMullen and Oxtoby,⁸⁸ Curtin^{91,92} examined the fcc (100) and (111) hard-sphere crystal/liquid interfaces. The theory predicted both interfaces to be about four lattice planes in width with $\gamma_{(111)} = 0.63kT/\sigma^2$ and $\gamma_{(100)} = 0.66kT/\sigma^2$. These values are more than a factor of 2 smaller than those predicted by McMullen and Oxtoby.^{88,89} Since the calculations differ in both the functional and the density parametrization used and no simulations exist for this system, it is difficult to comment on this discrepancy.

Table I. Summary of Crystal/Liquid Interface Simulations^a

system	ref(s)	(hkl)	T*	ρ_c^*	ρ_l^*	N	W_p	W_p in layers	W_D	W_D in layers	γ_d	
$(r/\sigma)^{-12}$	39,40	fcc (100)	2.0	1.427	1.374	7680	4-5 σ	6-7	3.5 σ	5	0.46(ϵ/σ^2) ^b	
	41	fcc (111)	-	-	-	6480	-	5	-	-	-	
$(r/\sigma)^{-6}$	25,43	bcc (100)	0.10	0.70	0.687	2160	5.7 σ	8	3.9 σ	5.5	-	
	25	bcc (100)	0.10	0.70	0.687	3430	6.4 σ	9	3.8 σ	5.4	-	
	25	bcc (110)	0.10	0.70	0.687	3500	9.0 σ	9	3.9 σ	3.8	-	
	25	bcc (111)	0.10	0.70	0.687	3600	7.0 σ	17	4.0 σ	9.8	-	
	LJ	26,45	fcc (100)	0.72	0.986	0.80	1500	7-8 σ	9-10	$\approx 4\sigma$	5	-
LJ	46	fcc (100)	1.15	1.024	0.941	1680	5 σ	6	-	-	-	
	47 ^c	fcc (100)	1.20	1.12	0.97	432	3 σ	4 ^d	-	-	-	
	48 ^{e,f}	hcp (0001)	0.70	1.33	-	860	-	-	-	-	-	
	49 ^{e,f}	hcp (0001)	0.70	1.33	-	4378	-	-	-	-	-	
	29,50	fcc (100)	0.67	0.963	0.818	1764	5-6 σ	6-8	3 σ	4	-	
	29,50	fcc (111)	0.67	0.963	0.818	1764	6-8 σ	(6-8)	3 σ	3	-	
	30,31,52	fcc (100)	0.617	0.946	0.828	1790	5 σ	7	3 σ	4	0.34(ϵ/σ^2) ^b	
	30,31,52	fcc (110)	0.617	0.945	0.830	1598	5 σ	9	3 σ	5	0.36(ϵ/σ^2) ^b	
	30,31,52	fcc (111)	0.617	0.944	0.823	1674	6 σ	7	3 σ	3	0.35(ϵ/σ^2) ^b	
	53	fcc (100)	1.14	1.024	0.936	35253	5 σ	7	-	-	-	
	53	fcc (111)	1.15	1.024	0.936	32353	6 σ	7	-	-	-	
	water (TIP4P)	57,58	ice 1h basal	240 K	0.0311 Å ⁻³	0.0341 Å ⁻³	8640	10-15 Å	5-8	≈ 10 Å	5	-
	water (SPC)	61	ice 1h basal	200 K	0.0311 Å ⁻³	0.0341 Å ⁻³	1440	10-15 Å	5-8	-	-	-
	silicon	27	dia. (100)	1760 K	0.0489 Å ⁻³	0.0533 Å ⁻³	≈ 1800	8Å	6	-	-	-
		27	dia. (111)	1760 K	0.0489 Å ⁻³	0.0533 Å ⁻³	≈ 1800	6Å	4	-	-	-
75 ^d		dia. (100)	1665 K	-	-	3456	g	-	-	-	-	
75 ^d		dia. (111)	1665 K	-	-	980	-	-	-	-	-	

^a For the width parameters, the numbers in parentheses represent the width in units of the lattice spacing. A dash indicates that the quantity was not calculated. Unless otherwise indicated, temperatures, and densities are given in the appropriate reduced units using parameters given in the text. ^b Surface stress was calculated. ^c Truncated LJ potential. ^d Potential energy profile width. ^e At least one static solid layer. ^f Modified LJ potential. ^g Interface faceted.

On the basis of the hard-sphere result, Curtin⁹² also used perturbation theory to calculate the interfacial free energy for the LJ fcc (111) interface under near triple point conditions, yielding a value of $0.43\epsilon/\sigma$. This estimate is not too different than the Broughton and Gilmer³¹ simulation value of $0.35\epsilon/\sigma$.

McMullen and Oxtoby⁹⁵ have also extended their formalism to include *molecular* systems. The approach is based on a spherical harmonic description of the orientational degrees of freedom of the molecules. The theory is relatively complex and was not applied to any specific system, but in principle could be applied to such systems as the ice/water interface and other liquid/crystal interfaces.

It should be noted that, with regard to density profiles, direct comparison of simulation and theory is, at present, hindered by the fact that the systems studied by each method form nonoverlapping sets. It would certainly be more useful to the progress of the field if future investigations were more closely coordinated.

Although the more recent density functional interface theories mentioned here give reasonable results for systems with short-ranged potentials such as the hard sphere and Lennard-Jones interactions, they cannot be applied to longer ranged systems whose equilibrium crystal structure at freezing is bcc. The reason for this is due not to flaws in the interface theories themselves, but rather to the difficulties in the application to a bcc system of the underlying freezing theories on which the interface theories are based.^{36,37} Hence, consistent boundary conditions for the interface calculation cannot be obtained, and direct comparison with the present simulations is not yet possible. The original DF calculations, which used just several Fourier components for simplicity, certainly need to be extended. It is hoped that the simulations reviewed here will provide both an incentive to explore further these theoretical

issues, and "experimental" data with which to test candidate theories.

VII. Summary

In sections IV and V above, we survey over 20 computer simulations of the equilibrium crystal/liquid interface. These simulations cover a variety of systems. To facilitate comparison, we summarize the principal results of these simulations in Table I.

A principal result of the simulations on simple systems is that the width and excess free energy of the interfacial region (measured from the diffusion and potential energy profiles) are relatively independent of the interfacial orientation. The apparent differences in the density profile widths among the various crystal faces are due primarily to differences in packing geometry and not to actual differences in the interfacial environment. For systems with directionally dependent interactions, such as water and silicon, the question of the degree of orientational dependence of the interfacial quantities remains open, due to the small number of simulations to date.

There are some outstanding unresolved issues. A general method for predicting the crystal/liquid surface free energy is lacking, despite the elegant method of "cleaving potentials" developed by Broughton and Gilmer.³¹ It is fair to say that a similar lack of technique exists for real experiments on crystal/liquid interfaces. At a lower level of importance, there are unresolved discrepancies concerning the existence or otherwise of islands of crystallike and liquidlike particles in snapshots of crystal/liquid interfaces. There is also a question of time scale for interchange between liquidlike and crystallike behavior (if it exists). This issue needs to be resolved in order to establish whether the properties of the system in the interface, which are unambiguously intermediate between crystal and liq-

uid, result from a time-average of crystal and liquid properties or (as we believe) from a uniform, time-independent region of the system that simply possesses intermediate properties. Finally, more detailed simulations of particle diffusion toward and away from the interface are clearly needed. With this foundation, rapid process in molecular level simulations of non-equilibrium interfaces seems probable. An immediate goal will be the heat flux profile for the moving interface near equilibrium.

Acknowledgments. This research was supported in part by the U.S. National Science Foundation through grant CHE-8913006 and in part by the Australian Research Council (ARC) (grant no. A29131271). A.D.J.H. thanks Professors D.W. Oxtoby and O. Karim for many discussions on interfaces.

References

- (1) Woodruff, D. P. *The Solid-Liquid Interface*; Cambridge University Press: London, 1973.
- (2) Glicksman, M. E.; Vold, C. *Acta Metall.* 1969, 17, 1.
- (3) Hardy, S. C. *Philos. Mag.* 1977, 35, 471.
- (4) Schaefer, R. J.; Glicksman, M. E.; Ayers, J. D. *Philos. Mag.* 1975, 32, 725.
- (5) Mutaftschiev, B.; Zell, J. *Surf. Sci.* 1968, 12, 317.
- (6) Grange, G.; Landers, R.; Mutaftschiev, B. *J. Cryst. Growth* 1980, 49, 343.
- (7) Turnbull, D. *J. Appl. Phys.* 1950, 21, 1022.
- (8) Bonissent, A. In *Interfacial Aspects of Phase Transitions*; Mutaftschiev, B., Ed.; D. Reidel Pub. Co.: Boston, 1982; p 143.
- (9) Gibbs, J. W. *The Collected Works*; Yale University Press: New Haven, 1957; Vol. 1.
- (10) Tiller, W. A. *The Science of Crystallization: Microscopic Interfacial Phenomena*; Cambridge University Press: New York, 1991.
- (11) Harrowell, P.; Oxtoby, D. W. *J. Chem. Phys.* 1984, 80, 1639.
- (12) Kirkwood, J. G.; Boggs, E. M. *J. Chem. Phys.* 1942, 10, 307.
- (13) Matsuguchi, M.; Aratono, M.; Motomura, K. *Bull. Chem. Soc. Jpn.* 1990, 63, 17.
- (14) Goh, M. C.; Hicks, J. M.; Kemnitz, J.; Pinto, G. R.; Eiselthal, K. B.; Heinz, T. F. *J. Chem. Phys.* 1988, 92, 5074.
- (15) Swope, W. C.; Anderson, H. C. *Phys. Rev. B* 1990, 41, 7042.
- (16) Metropolis, N.; Rosenbluth, A. W.; Rosenbluth, M. N.; Teller, A. H. *J. Chem. Phys.* 1953, 21, 1087.
- (17) Alder, B. J.; Wainwright, T. E. *J. Chem. Phys.* 1957, 27, 1208.
- (18) Allen, M. A.; Tildesley, D. J. *Computer Simulation of Liquids*; Oxford Science Press: Oxford, 1987.
- (19) Hansen, J. P.; Velet, L. *Phys. Rev.* 1969, 184, 151.
- (20) Hansen, J. P. *Phys. Rev. A* 1970, 2, 221.
- (21) Hansen, J. P. *Mol. Phys.* 1973, 25, 1281.
- (22) Hoover, W. G.; Ross, M.; Johnson, K. W.; Henderson, D.; Barker, J. A.; Brown, B. C. *J. Chem. Phys.* 1970, 52, 4931.
- (23) Hoover, W. G.; Gray, S. G.; Johnson, K. W. *J. Chem. Phys.* 1971, 55, 1128.
- (24) Stringfellow, G. S.; DeWitt, H. E.; Slattery, W. L. *Phys. Rev. A* 1990, 41, 1105.
- (25) Laird, B. B.; Haymet, A. D. J. *Mol. Phys.* 1992, 75, 71.
- (26) Ladd, A. J. C.; Woodcock, L. V. *Chem. Phys. Lett.* 1977, 51, 155.
- (27) Abraham, F. F.; Broughton, J. Q. *Phys. Rev. Lett.* 1986, 56, 734.
- (28) Laird, B. B.; Haymet, A. D. J. *J. Chem. Phys.* 1989, 91, 3638.
- (29) Broughton, J. Q.; Bonissent, A.; Abraham, F. F. *J. Chem. Phys.* 1981, 44, 4029.
- (30) Broughton, J. Q.; Gilmer, G. H. *Acta Metall.* 1983, 31, 845.
- (31) Broughton, J. Q.; Gilmer, G. H. *J. Chem. Phys.* 1986, 84, 5759.
- (32) Bernal, J. D. *Nature* 1959, 183, 141.
- (33) Finney, J. L. *J. Phys. (Paris)* 1975, 36, C2-1.
- (34) Zell, J.; Mutaftschiev, B. *J. Cryst. Growth* 1972, 13/14, 231.
- (35) Bonissent, A.; Mutaftschiev, B. *Philos. Mag.* 1977, 35, 65.
- (36) Barrat, J. L.; Hansen, J. P.; Pastore, G.; Waisman, E. M. *J. Chem. Phys.* 1987, 86, 6360.
- (37) Laird, B. B.; Kroll, D. M. *Phys. Rev. A* 1990, 42, 4810.
- (38) Young, D. A. *Phase Diagrams of the Elements*; University of California Press: Berkeley, 1991.
- (39) Cape, J. N.; Woodcock, L. V. *Chem. Phys. Lett.* 1978, 59, 271.
- (40) Cape, J. N.; Woodcock, L. V. *J. Chem. Phys.* 1980, 80, 2420.
- (41) Tallon, J. *Phys. Rev. Lett.* 1986, 57, 1328.
- (42) Swope, W. C.; Anderson, H. C.; Berens, P. H.; Wilson, K. R. *J. Chem. Phys.* 1982, 76, 637.
- (43) Laird, B. B.; Haymet, A. D. J. *Mater. Res. Soc. Symp. Proc.* 1986, 63, 67.
- (44) Lennard-Jones, J. E. *Physica* 1937, 4, 941.
- (45) Ladd, A. J. C.; Woodcock, L. V. *J. Phys. C* 1978, 11, 3565.
- (46) Torvaerd, S.; Praestgaard, E. *J. Chem. Phys.* 1977, 67, 5291.
- (47) Hiwatari, Y.; Stoll, E.; Schneider, T. *J. Chem. Phys.* 1978, 68, 3401.
- (48) Bonissent, A.; Gauthier, E.; Finney, J. L. *Philos. Mag.* 1979, 39, 49.
- (49) Bushnell-Wye, G.; Finney, J. L.; Bonissent, A. *Philos. Mag.* 1981, 44, 1053.
- (50) Broughton, J. Q.; Abraham, F. F. *Chem. Phys. Lett.* 1983, 71, 456.
- (51) Landman, U.; Barnett, R. N.; Cleveland, C. L.; Rast, R. H. *J. Vac. Sci. Technol.* 1984, A3, 1574.
- (52) Broughton, J. Q.; Gilmer, G. H. *J. Chem. Phys.* 1986, 84, 5749.
- (53) Galejs, R. J.; Raveché, H. J.; Lie, G. *Phys. Rev. A* 1989, 39, 2574.
- (54) Vlachy, V.; Haymet, A. D. J. *J. Chem. Phys.* 1986, 74, 2559.
- (55) Wong, C. F.; McCammon, J. A. *Israel J. Chem.* 1986, 27, 211.
- (56) Spohr, E.; Heinzinger, K. *Chem. Phys. Lett.* 1986, 123, 218.
- (57) Karim, O. A.; Haymet, A. D. J. *Chem. Phys. Lett.* 1987, 138, 531.
- (58) Karim, O. A.; Haymet, A. D. J. *J. Chem. Phys.* 1988, 89, 6889.
- (59) Jorgensen, W. L.; Chandrasekhar, J.; Madura, J. D.; Impey, R. W.; Klein, W. L. *J. Chem. Phys.* 1983, 79, 926.
- (60) Jorgensen, W. L.; Madura, J. D. *Mol. Phys.* 1985, 56, 1381.
- (61) Karim, O. A.; Kay, P. A.; Haymet, A. D. J. *J. Chem. Phys.* 1990, 92, 4634.
- (62) Berendsen, J. C.; Postma, J. P. M.; van Gunsteren, W. F.; Hermans, J. In *Intermolecular Forces*; Pullmann, B., Ed.; Reidel: Dordrecht, 1981; p 331.
- (63) Kuhs, W. F.; Lehmann, M. S. In *Water Science Reviews 2*; Franks, F., Ed.; Cambridge University Press: New York, 1986; p 1.
- (64) Narten, A. H.; Levy, H. A. *J. Chem. Phys.* 1971, 55, 2263.
- (65) Soper, A. K.; Phillips, M. G. *Chem. Phys.* 1986, 107, 47.
- (66) Shen, Y. R. *J. Vac. Sci. Technol.* 1985, B3, 1464.
- (67) Rasing, T.; Shen, Y. R.; Kim, M. W.; Valint, P., Jr.; Bock, J. *Phys. Rev. A* 1985, 31, 537.
- (68) Hicks, J. M.; Kemnitz, K.; Eiselthal, K. B.; Heinz, T. F. *J. Chem. Phys.* 1986, 90, 560.
- (69) Beaglehole, D.; Nason, D. *Surf. Sci.* 1980, 96, 357.
- (70) Brown, R. A.; Kelzer, J.; Stelger, U.; Yeh, Y. *J. Phys. Chem.* 1983, 87, 4135.
- (71) Guttinger, H.; Bilgram, J. H.; Kanzig, W. *J. Phys. Chem. Solid* 1979, 40, 55.
- (72) Bilgram, J. H. In *Nonlinear phenomena at phase transition instabilities*; Riste, T., Ed.; Plenum Press: New York, 1982; p 343.
- (73) Ryckaert, J. P.; Ciccotti, G.; Berendsen, H. J. C. *J. Comput. Phys.* 1977, 23, 327.
- (74) Broughton, J. Q.; Gilmer, G. H. *J. Phys. Chem.* 1987, 91, 6347.
- (75) Stillinger, F. H.; Weber, T. A. *Phys. Rev. B* 1985, 31, 5262.
- (76) Landman, U.; Luedtke, W. D.; Barnett, R. N.; Cleveland, C. L.; Ribarsky, M. W.; Arnold, E.; Ramesh, S.; Baumgart, H.; Martinez, A.; Khan, B. *Phys. Rev. Lett.* 1986, 56, 155.
- (77) Jackson, K. A. *Liquid Metals and Solidification*; ASM: Cleveland, 1958.
- (78) Cahn, J. W.; Hilliard, J. E. *J. Chem. Phys.* 1959, 28, 258.
- (79) Evans, R. *Adv. Phys.* 1979, 28, 143.
- (80) Mermin, N. D. *Phys. Rev.* 1965, 137, A1441.
- (81) Laird, B. B.; McCoy, J. D.; Haymet, A. D. J. *J. Chem. Phys.* 1987, 87, 5449.
- (82) Haymet, A. D. J. *Annu. Rev. Phys. Chem.* 1987, 38, 89.
- (83) Baus, M. *J. Phys.: Condens. Matter* 1987, 2, 2111.
- (84) Singh, Y. *Phys. Rep.* 1991, 207, 351.
- (85) Haymet, A. D. J.; Oxtoby, D. W. *J. Chem. Phys.* 1981, 74, 2559.
- (86) Ramakrishnan, T. V.; Yussouff, R. *Phys. Rev. B* 1979, 19, 2775.
- (87) Moore, S. M.; Raveché, H. R. *J. Chem. Phys.* 1986, 85, 6039.
- (88) McMullen, W. E.; Oxtoby, D. W. *J. Chem. Phys.* 1988, 88, 1967.
- (89) Oxtoby, D. W.; McMullen, W. E. *Phys. Chem. Liq.* 1988, 18, 97.
- (90) Mikheev, L.; Trayanov, A. *Surf. Sci.* 1989, 223, 299.
- (91) Curtin, W. A. *Phys. Rev. Lett.* 1987, 59, 1228.
- (92) Curtin, W. A. *Phys. Rev. B* 1989, 39, 6775.
- (93) Curtin, W. A.; Ashcroft, N. W. *Phys. Rev. A* 1985, 32, 2909.
- (94) Tarazona, P. *Mol. Phys.* 1984, 52, 81.
- (95) McMullen, W. E.; Oxtoby, D. W. *J. Chem. Phys.* 1988, 88, 7757.

Registry No. H₂O, 7732-18-5; Si, 7440-21-3.